Biol Cybern (2009) 100:159–184
DOI 10.1007/s00422-008-0287-0

ORIGINAL PAPER

Biological Cybernetics

Parabolic movement primitives and cortical states: merging optimality with geometric invariance

Felix Polyakov · Eran Stark · Rotem Drori · Moshe Abeles · Tamar Flash

Received: 4 July 2008 / Accepted: 15 December 2008 / Published online: 17 January 2009

Abstract Previous studies have suggested that several types of rules govern the generation of complex arm movements. One class of rules consists of optimizing an objective function (e.g., maximizing motion smoothness). Another class consists of geometric and kinematic constraints, for instance the coupling between speed and curvature during drawing movements as expressed by the two-thirds power law. It has also been suggested that complex movements are composed of simpler elements or primitives. However, the ability to unify the different rules has remained an open problem. We address this issue by identifying movement paths whose generation according to the two-thirds power law yields maximally smooth trajectories. Using equi-affine differential geometry we derive a mathematical condition which these paths must obey. Among all possible solutions only parabolic paths minimize hand jerk, obey the two-thirds power law and are invariant under equi-affine transformations (which preserve the fit to the two-thirds power law). Affine transformations can be used to generate any parabolic stroke from an arbitrary parabolic template, and a few parabolic strokes may be concatenated to compactly form a complex path. To test the possibility that parabolic elements are used to generate planar movements, we analyze monkeys' scribbling trajectories. Practiced scribbles are well approximated by long parabolic strokes. Of the motor cortical neurons recorded during scribbling more were related to equi-affine than to Euclidean speed. Unsupervised segmentation of simultaneously recorded multiple neuron activity yields states related to distinct parabolic elements. We thus suggest that the cortical representation of movements is state-dependent and that parabolic elements are building blocks used by the motor system to generate complex movements.

Keywords Drawing primitives · Equi-affine geometry · Geometric invariants · Neural representation · Hidden Markov modeling

F. Polyakov (✉) · T. Flash
Department of Computer Science and Applied Mathematics, Weizmann Institute of Science, 76100 Rehovot, Israel
e-mail: felix.polyakov@weizmann.ac.il

E. Stark · R. Drori · M. Abeles
Department of Physiology, Hadassah Medical School, Hebrew University, 91120 Jerusalem, Israel

M. Abeles
Gonda Brain Research Center, Bar-Ilan University, 52900 Ramat-Gan, Israel

1 Introduction

Elementary biological movements follow stereotypical patterns. For example, despite the large variety of hand movements that humans and monkeys can generate, point-to-point movements tend to be nearly straight and have bell-shaped tangential velocity profiles (Morasso 1981). Several models have been developed to account for the observed features of human movements.

One family of models used in the description of arm trajectories is based on optimality principles, the idea that movements are selected to optimize a particular cost function (Todorov 2004; Kording and Wolpert 2006). The minimum-jerk model is based on minimizing a kinematic cost function. The model predicts maximally smooth trajectories, accounting for multiple kinematic features of single-joint movements (Hogan 1984), of two-joint movements (Flash and Hogan 1985) and of movements that follow prescribed geometrical paths (the constrained minimum-jerk model, (Viviani and Flash 1995; Todorov and Jordan 1998; Richardson and Flash 2002)). Other models have optimized parameters including

muscle forces (Uno et al. 1989; Nakano et al. 1999), feedback control (Todorov and Jordan 2002; Scott 2004), movement accuracy (Harris and Wolpert 1998; Osu et al. 2004), or a trade-off between movement accuracy and duration (Harris and Wolpert 2006; Tanaka et al. 2006).

A different and plausible strategy for constructing complex biological movements is combining several basic motion elements or movement "primitives" into more complex movements. Primitives may exist at the kinetic, kinematic and/or neural levels of the motor system (Mussa-Ivaldi and Solla 2004; Flash and Hochner 2005; Giszter et al. 2007). A kinematic constraint, the two-thirds power law, indicated segmented control of drawing movements (Viviani 1986). This empirical law formalizes a piecewise constant relationship between angular velocity and path curvature (Lacquaniti et al. 1983). The two-thirds power law was also demonstrated in visual perception studies (Viviani and Stucchi 1992; Levit-Binnun et al. 2006; Dayan et al. 2007).

A fundamental open question is which geometric properties of movements are selected by the motor system for planning and executing movements: "The constrained minimum-jerk model and the power law predict similar speed profiles for a given path. There seem to exist a family of paths for which the two are exactly equivalent and identifying that family may provide further insights" (Todorov and Jordan 1998). The first objective of this work is to identify geometric properties of movement paths for which the two-thirds power law and the constrained minimum-jerk model can be satisfied simultaneously.

If complex movements are composed of primitives, reducing their number to a minimum may reduce computational and memory load. Invariance of motion primitives with respect to some geometric or temporal transformations may reduce the dimensionality of the space needed for movement representation (Polyakov 2001, 2006). Early studies showed that the velocity and curvature profiles of human hand trajectories are invariant under Euclidean transformations (translation and rotation; e.g., Flash and Hogan 1985). However, the two-thirds power law is invariant under a larger class of geometric transformations, namely equi-affine transformations (Pollick and Sapiro 1997; Handzel and Flash 1999; Flash and Handzel 2007).

Equi-affine transformations are a subgroup of affine transformations that preserve parallelism between lines and conserve area. Thus, our second objective is to identify geometric movement primitives which are invariant under equi-affine transformations (Polyakov 2001).

Our third objective is to assess the representation of equi-affine geometry and geometric movement primitives in motor cortical activity during movement. In a recent human fMRI study Dayan et al. (2007), demonstrated that brain activity during observation of movements following the two-thirds power law is much stronger and more widespread than brain activity during other types of motion. In earlier monkey studies of movement production, activity of primary motor and dorsal premotor cortical neurons was correlated with the Euclidian speed of hand trajectories during point-to-point and tracking movements (Schwartz 1992; Moran and Schwartz 1999; Johnson et al. 1999; Paninski et al. 2004). The possibility that equi-affine speed is represented in the activity of motor cortical neurons has not yet been systematically investigated. We thus analyzed well practiced monkey scribbling movements (not constrained by any explicit cue) and the simultaneously recorded activity of motor cortical neurons (see also Polyakov 2006). To estimate the influence of Euclidian and equi-affine speeds on the variability of single-unit firing rates, we adopted the approach developed by Stark et al. (2007).

Different movement primitives may be associated with separate states of cortical activity. The idea of state-dependent information processing in the cortex is related to the cell-assembly hypothesis (Hebb 1949) and supported by a number of empirical studies (e.g., Abeles et al. 1995; Kenet et al. 2003; Jackson et al. 2006; Jones et al. 2007). Repetitive stimulation of specific sensory receptors is postulated to lead to the formation of cell assemblies, which act briefly as closed systems after stimulation has ceased. Analogously, repeated performance of stereotypical movements, or primitives, may be related to the formation of assemblies of motor cortical cells, which may coherently switch between different states when different primitives are executed. To study this possibility, we used hidden Markov modeling to partition the activity of multiple neurons recorded simultaneously into network states in an unsupervised way, without any information about the movement (Gat and Tishby 1993; Abeles et al. 1995).

2 Mathematical background and methods

2.1 Equi-affine geometric invariants and the special role of parabolas in equi-affine geometry

Since invariants of equi-affine transformations are used throughout, we begin by briefly introducing relevant notions from equi-affine geometry (for further details on equi-affine geometry, see Handzel and Flash 1999; Polyakov 2006; Flash and Handzel 2007). For an extensive mathematical background for differential geometry see Shirokov and Shirokov (1959); Guggenheimer (1977) and Spivak (1999).

Planar affine transformations,

$$\begin{pmatrix} x^* \\ y^* \end{pmatrix} = A \cdot \begin{pmatrix} x \\ y \end{pmatrix} + \begin{pmatrix} a \\ b \end{pmatrix}, \quad \text{where } A = \begin{pmatrix} \alpha & \beta \\ \gamma & \delta \end{pmatrix}, \quad (1)$$

which are constrained by the condition $\det A = 1$, are called equi-affine. The transformation includes a linear part defined

by three independent terms appearing in matrix A; the fourth term depends on the other three due to the condition $\det A = 1$. It also includes a translation based on the constants a and b. The variables x and y are coordinates of a point on a curve, and x^* and y^* are the coordinates of the same point following the transformation. The condition on the determinant means that the area contained within any closed curve is conserved under equi-affine transformations; these transformations are therefore also called area-preserving.

The set of Euclidian transformations consists of rigid rotations and translations that preserve Euclidian distance and curvature, and constitutes a particular subset of equi-affine transformations. An equi-affine transformation can be applied to all points of a curve. The Euclidian length of a curve and its Euclidian curvature are modified correspondingly (Fig. 1). However, the equi-affine length and the equi-affine curvature, defined below, remain the same.

We use the notion of trajectories as time-dependent functions defining motion along a given geometric object, a path. Consider a twice differentiable planar trajectory described by the vector function $\mathbf{r}(t) = \{x(t), y(t)\}$ (throughout, bold-faced symbols signify vector quantities, and a dot above a symbol denotes a time derivative). Its equi-affine velocity, which equals the time derivative of the equi-affine arc-length σ, is invariant under equi-affine transformations and is expressed as (Shirokov and Shirokov 1959; Guggenheimer 1977):

$$\dot{\sigma}(t) = \sqrt[3]{\dot{x}(t)\,\ddot{y}(t) - \dot{y}(t)\,\ddot{x}(t)}. \tag{2}$$

For a given curve, this formula corresponds to the first order form of a differential expression which is invariant under equi-affine transformations of the coordinate system, like the Euclidian invariant measurement $\dot{s} = \sqrt{\dot{x}^2 + \dot{y}^2}$. The mathematical framework for the invariant differential form underlying the equi-affine velocity can be found in Shirokov and Shirokov (1959). (For an English translation of the relevant text see Polyakov 2006, pp. 165–174).

To gain an intuitive understanding of the properties of the expression for equi-affine velocity in Eq. (2), we note that the expression $\dot{x}\ddot{y} - \dot{y}\ddot{x}$ represents the area of the parallelogram defined by the velocity and acceleration vectors and is therefore invariant under equi-affine transformations. Given the expression $\dot{x}\ddot{y} - \dot{y}\ddot{x}$, assume that some trajectory is drawn a times faster than its original speed, so that the new trajectory is $\tilde{\mathbf{r}}(t) = \mathbf{r}(at)$. This implies that $\dddot{\tilde{x}}\ddot{\tilde{y}} - \dddot{\tilde{y}}\ddot{\tilde{x}} = a^3\left[dx/d\tau d^2y/d\tau^2 - dy/d\tau d^2x/d\tau^2\right]\big|_{\tau=at}$. Taking the cubic root of the above equality we obtain $\sqrt[3]{\dddot{\tilde{x}}\ddot{\tilde{y}} - \dddot{\tilde{y}}\ddot{\tilde{x}}} = a\sqrt[3]{dx/d\tau d^2y/d\tau^2 - dy/d\tau d^2x/d\tau^2}\Big|_{\tau=at}$, or $\dot{\tilde{\sigma}} = a\, d\sigma/d\tau|_{\tau=at}$. Thus, a correct rescaling of the equi-affine velocity is achieved by taking the cubic root of $\dot{x}\ddot{y} - \dot{y}\ddot{x}$. Equation (2) implies that the equi-affine length is measured in (Euclidian distance units)$^{2/3}$ such as (mm)$^{2/3}$ as opposed to Euclidian distance which is measured in mm.

For a trajectory $\mathbf{r}(t)$ without inflection points (points where the Euclidian curvature is zero), parameterized by the equi-affine arc length σ (also called "natural parameterization"), a derivative w.r.t. σ is denoted by prime, $x' = dx(t(\sigma))/d\sigma = \dot{x}/\dot{\sigma}$, where $t(\sigma)$ corresponds to the movement duration during which an equi-affine distance σ mm$^{2/3}$ of the path is drawn. The following condition of equi-affine parameterization holds:

$$x'y'' - y'x'' = 1. \tag{3}$$

Equation (3) corresponds to the area spanned by the equi-affine tangent $(\mathbf{r}')$ and the equi-affine normal $(\mathbf{r}'')$ to the curve and is invariant under equi-affine transformations. The expression in Eq. (3) is equal to the outer product and not to the scalar product of the two vectors.

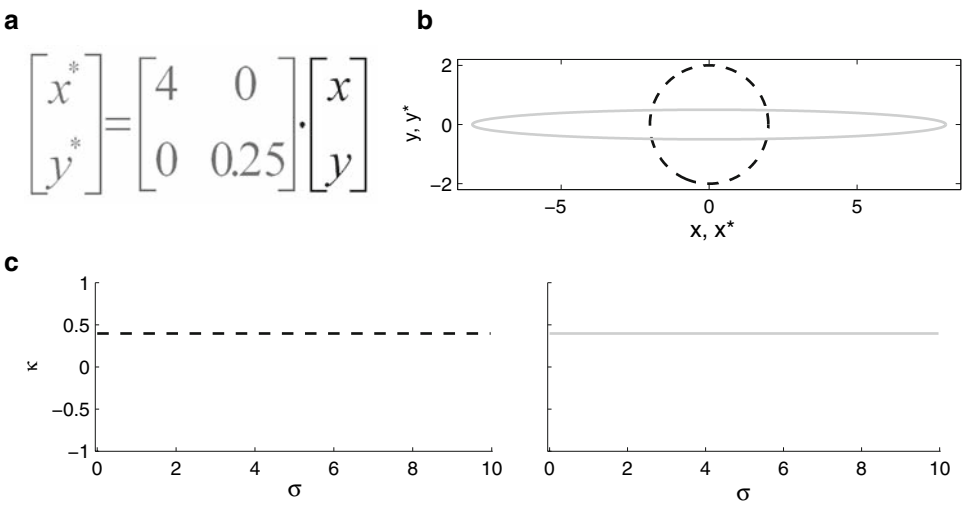

Fig. 1 Illustration of equi-affine transformations. **a** An example of an equi-affine transformation. **b** The transformation is applied to the circle (*dashed line*), resulting in an ellipse (*continuous line*). Both shapes enclose the same area, have the same equi-affine curvature, and can be aligned by the equi-affine transformation shown in **a**. **c** The equi-affine curvature of the circle as a function of the equi-affine length (*left*) is equal to the equi-affine curvature of the ellipse (*right*) because one is an equi-affine image of the other

Differentiation of Eq. (3) with respect to σ shows that the vectors corresponding to the first and the third derivatives of the position vector are parallel to each other and can thus always be related to each other by multiplying one of the vectors by the scalar:

$$\mathbf{r}''' + \kappa \mathbf{r}' = 0, \tag{4}$$

with the proportionality coefficient κ obtained from Eqs. (3) and (4) by

$$\kappa(\sigma) = x''y''' - y''x'''. \tag{5}$$

The coefficient κ is the equi-affine curvature of a curve (Shirokov and Shirokov 1959; Guggenheimer 1977), which is the second equi-affine invariant that we use (the first is the equi-affine length or its time-derivative equi-affine velocity). Given an analytical expression of a trajectory parameterized by time, its equi-affine curvature can be computed directly without using natural parameterization according to Eq. (A6) in Appendix A. Eqs. (5) and (A6) include high-order derivatives, making it impractical to estimate equi-affine curvature from empirical data. Fortunately, an approximation based on conics has been proposed (Calabi et al. 1998).

The equi-affine curvature can be used for characterizing and classifying planar curves. This is justified by the main theorem of the equi-affine theory of planar curves, stating that "The natural equation $\kappa(\sigma) = f(\sigma)$ defines a planar curve up to an arbitrary equi-affine transformation" (Shirokov and Shirokov 1959). This theorem implies that whenever two curves can be co-aligned by an equi-affine transformation, their equi-affine curvatures are equal, that is, $\kappa_1(\sigma) = \kappa_2(\sigma)$ for every σ (and vice versa). For example, the circle and the ellipse depicted in Fig. 1b are identical in equi-affine geometry, since each is an equi-affine image of the other; consequently both have the same equi-affine arc-length and curvature.

Three classes of curves with constant equi-affine curvature can be obtained from Eq. (4). These curves constitute conic sections: ellipses, hyperbolas, and parabolas. Ellipses have positive constant equi-affine curvature and are described by

$$\mathbf{r}(\sigma) = \frac{1}{\sqrt{\kappa}}\left(\mathbf{a}\sin\left(\sqrt{\kappa}\sigma\right) + \mathbf{b}\cos\left(\sqrt{\kappa}\sigma\right)\right) + \mathbf{r_0},$$

with $\sqrt{k}\left(a_x b_y - b_x a_y\right) = -1$ (Shirokov and Shirokov 1959; Guggenheimer 1977). Hyperbolas have negative constant equi-affine curvature and are expressed as follows:

$$r(\sigma) = \frac{1}{\sqrt{-\kappa}}\left(\mathbf{a}\sinh\left(\sqrt{-\kappa}\sigma\right) + \mathbf{b}\cosh\left(\sqrt{-\kappa}\sigma\right)\right) + \mathbf{r_0},$$

with $\sqrt{-\kappa}\left(a_x b_y - b_x a_y\right) = 1$ (Shirokov and Shirokov 1959; Guggenheimer 1977). The constant vectors $\mathbf{a}$ and $\mathbf{b}$ correspond to the symmetry lines of the ellipses and hyperbolas, and $\mathbf{r_0}$ is the center of a shape.

Parabolas have zero equi-affine curvature and are described by the following general equation:

$$\mathbf{r}(\sigma) = \mathbf{a}\sigma^2 + \mathbf{b}\sigma + \mathbf{c} \tag{6}$$

with the condition $2\left(a_x b_y - b_x a_y\right) = -1$. The symmetry line of such a parabola is parallel to the constant vector $\mathbf{a}$ (Shirokov and Shirokov 1959; Guggenheimer 1977).

Apart from their zero equi-affine curvature, parabolas have additional special properties in equi-affine geometry. They are equi-affine geodesics maximizing the equi-affine length among all convex curves which connect two points, have prescribed tangent directions at those points, and do not have tangent directions outside the interval defined by the directions at the two end-points (Calabi et al. 1996; Handzel and Flash 2001; Flash and Handzel 2007).

2.2 The two-thirds power law, the minimum-jerk model, and equi-affine invariant parameters

We use two models: the two-thirds power law (Lacquaniti et al. 1983) and the constrained minimum-jerk model (Todorov and Jordan 1998). Let $\mathbf{r}(s(t)) = \{x(s(t)), y(s(t))\}$ be a planar trajectory describing hand movement during a particular trial, where s is the Euclidean distance along the curve and $\dot{s}(t) = \sqrt{\dot{x}^2(t) + \dot{y}^2(t)}$ is the hand's tangential velocity (Euclidian speed). The constrained minimum-jerk model assumes that motion along a prescribed geometrical path with total duration T is defined by a scalar function $s(t)$ which minimizes the integrated jerk, namely $J = \frac{1}{2}\int_0^T \left\{\dddot{x}^2[s(t)] + \dddot{y}^2[s(t)]\right\} dt$. Put in vector form

$$J = \frac{1}{2}\int_0^T \left\|\dddot{\mathbf{r}}[s(t)]\right\|^2 dt, \text{ provided } \mathbf{r}(s). \tag{7}$$

In the original formulation of the minimum-jerk model (Hogan 1984; Flash and Hogan 1985), both path and speed were predicted for a set of specified initial, via, and final positions and for prescribed velocities and accelerations at the end-points. Because the path is explicitly specified and minimization is performed over all possible speed profiles, the formulation in Eq. (7) differs from the original one.

The two-thirds power law formalizes the relationship between the angular velocity A and the Euclidian curvature c during movement along a given path: $A = Kc^{2/3}$. The velocity gain factor K is piece-wise constant (Lacquaniti et al. 1983). Noting that $A = \dot{s}c$, an equivalent relation based on the tangential instead of angular velocity is (Viviani and Cenzato 1985)

$$\dot{s} = Kc^{-1/3}. \tag{8}$$

The two-thirds power law can be formulated in equi-affine terms, noting that K in Eq. (8) is exactly the equi-affine

velocity $\dot{\sigma}$ (Pollick and Sapiro 1997; Handzel and Flash 1999; Flash and Handzel 2007):

$$K = \dot{s}c^{1/3} = \sqrt[3]{\dot{x}\dddot{y} - \ddot{x}\ddot{y}} = \dot{\sigma}. \quad (9)$$

Thus, for a movement that satisfies the two-thirds power law, the equi-affine velocity $\dot{\sigma}$ is piece-wise constant, since K is piece-wise constant and therefore its absolute value $|\dot{\sigma}|$, namely the equi-affine speed, is also piece-wise constant. The trajectories obtained after applying equi-affine transformations to movements obeying the two-thirds power law still comply with the two-thirds power law, because equi-affine velocity is invariant under equi-affine transformations.

The relationship in Eq. (9) helps to establish a connection between the equi-affine length σ of a curve and its Euclidian invariants:

$$\sigma(t) = \int_0^{L(t)} c^{1/3}(s)\mathrm{d}s,$$

where $L(t)$ is the Euclidian length of the trajectory from the start to the point $\mathbf{r}(t)$. This means that the equi-affine length of a curve is equal to the Euclidian length weighted by the cubic root of the Euclidian curvature along the curve.

2.3 Data recording procedure

To assess the use of parabolic movement elements to construct complex movements we analyzed monkeys' spontaneous planar scribbling movements (female *Macaca fascicularis*; monkeys O and U). In monkey U concurrent motor cortical activity was analyzed. Movements were recorded during several consecutive sessions from the start of practice. The monkeys operated a horizontal planar manipulandum using their right hands; an opaque white plate blocked their view of the manipulandum and arm, the monkeys seeing only the cursor. When the manipulandum end-point was moved into an invisible target, the monkey was rewarded by a drop of juice. Immediately, another target was randomly selected and the process was repeated. For details of the experimental setup and the neural recording procedure for monkey U, see Stark et al. (2007). A total of 19 targets were tiled symmetrically—hexagons for monkey U and an equivalent set of circles for monkey O.

2.4 Testing parabolic features of the recorded trajectories

To test empirically whether parabolas constitute movement primitives we fitted parabolic elements to strokes of recorded trajectories and analyzed the geometrics features of these elements.

First, drawn trajectories were segmented into periods of active motion and rest. Segments during which the tangential velocity was greater than a threshold of 150 mm/s were classed as "active motion". Portions of the trajectory whose tangential velocity was slower than this threshold for at least 0.2 s were defined as "rest". This resulted in segments of active motion separated by segments of rest. The identified motion segments were prolonged for 0.1 s forward and backward in time or until the closest minima in the tangential velocity, whichever came first. Motion segments were then segmented into separate strokes, a stroke lying between local minima of Euclidian curvature, i.e., each stoke contained a single maximum of Euclidian curvature. Every stroke was fitted with a parabolic element (by minimizing the cost D defined below, using the *fminsearch* routine; MATLAB). This was subsequently rotated and translated into its canonical representation, $y = x^2/(2p)$. The parameter p is the focal parameter of the fitted parabola and is equal to the radius of curvature at the point of maximal curvature of the parabola. The same Euclidian transformation was applied to the original stroke so the recorded (x_i, y_i) and modeled $(x_i, \tilde{y}_i)$ position samples were considered within the canonical coordinate system (the x coordinates of the original and modeled samples are the same ($\tilde{x} = x$)). The error of fitting a stroke was estimated by the proportion of data variance unexplained by the parabolic model:

$$D = 1 - R^2 = \frac{\sum\left(y_i - x_i^2/(2p)\right)^2}{\sum\left[(x_i - \mathrm{mean}(x))^2 + (y_i - \mathrm{mean}(y))^2\right]}.$$

Note that the fitting procedure does not fit the motion segments with a large number of arbitrary short parabolas: if the fit was bad (e.g., $D > 0.01$), the element of path being fitted is not split further into smaller parts. The median duration of fitted parabolic strokes was 0.25 s and median length was 70 mm.

To quantify the closeness of the equi-affine curvature to zero we calculated the median absolute value of the equi-affine curvature $|\kappa|$ from Eq. (5) and its median absolute deviation: $\mathrm{MAD}(|\kappa|) = \mathrm{median}(|\mathrm{median}(|\kappa|) - |\kappa||)$. This was done for periods of active motion separately for each session. The MAD is a non-parametric measure of how close values are to their median. Median values were used because numerical estimation of equi-affine curvature contains outliers (see also the high-order differentiation in Eq. (5) and (A6)).

Parabolas in the canonical coordinate system are expressed as second order polynomials when parameterized by the abscissa: $y = x^2/(2p)$. We therefore tested the degree of fit of higher order polynomials parameterized by x in the same coordinate system. The parabolic fit was also compared with the fit based on other geometric representations including ellipses and triplets of superimposed point-to-point movements. The quantitative comparison of the fit to different geometric shapes was based on the trade-off between the goodness-of-fit and simplicity (number of parameters) of the fitted curve. The test is based on the Schwarz informa-

tion criterion (SIC; also known as the Bayesian information criterion, BIC), which is an extension of Akaike's maximum likelihood criterion (Schwarz 1978). To conform to the idea of a model as a distribution, we considered the density function (or likelihood) defined by the dimensionless quadratic estimate of the deviation from the model $\left(1-R^2\right)$:

$$P\left(\text{movement stroke} \mid \text{model}\right) = \frac{1}{\left(2\pi\right)^{-n/2}} e^{-\left(1-R^2\right)/\left(2R^2\right)},$$

where n is the number of the recorded data samples which define a movement stroke (stroke duration multiplied by the recording frequency). The value of P is highest in case of an ideal fit $\left(R^2=1\right)$ and lowest when R^2 is close to zero. We then considered the SIC score (Schwarz 1978)

$$SIC = \log P - \frac{1}{2} k \log n,$$

where k is the number of parameters in the model. The optimal model here (goodness-of-fit vs. simplicity tradeoff) corresponds to the maximal value of the SIC score.

To assess whether greater smoothness per se implies piecewise parabolic trajectories, we simulated smooth trajectories using the minimum-jerk model with multiple via-points, without a priori assuming curvature-speed coupling as prescribed by the two-thirds power law (Todorov and Jordan 1998; for details see Polyakov 2001, pp. 33–36, 77–80). End-points of a movement segment, potentially containing several parabolic elements, were used as end-points of the simulated trajectory. Points of local maxima of Euclidean curvature, which correspond to the vertices of the fitted parabolas, were used as via-points (Reina and Schwartz 2003). Velocity and acceleration at the end-points of the simulated trajectories were set to zero (periods of rest separate movement segments).

Next, for the simulated smooth paths, we identified pairs of consecutive local minima of Euclidian curvature with a via-point between them. Parabolas were fitted to the simulated strokes in the same manner as to the drawn paths. A parabolic stroke is characterized by a global maximum of Euclidian curvature at its vertex, and every parabolic stroke containing a vertex is characterized by a minimum–maximum–minimum pattern of Euclidian curvature. Therefore, the piecewise parabolic structure of the drawn and simulated movements was assessed using the differences between the maximal and minimal values of Euclidian curvature for each path stroke fitted with a parabola.

2.5 Representation of movement speeds in the activity of motor cortical neurons

Here we describe the procedure used to compare representation strength of Euclidian and equi-affine invariant speeds (magnitudes of the velocity vector) in motor cortical activity during well-trained movements. Equi-affine speed $|\dot{\sigma}|$ and Euclidian speed $\dot{s}$ of practiced scribbles are smooth (so the cubic root of the Euclidian curvature c changes relatively little). The movements mostly also have the same orientation (counter clock-wise for monkey U), thus reducing the number of inflection points at which $c=0$. These considerations explain in part the high correlation in our data between the equi-affine and Euclidian speeds (as implied by Eq. (8), namely $|\dot{\sigma}| = \dot{s}\,|c|^{1/3}$), with a peak correlation coefficient of 0.8 ± 0.03 (mean $\pm$ SD over 17 sessions). The lag of the peak was 52 ± 13 ms (mean $\pm$ SD over 17 sessions). Therefore, neural activity related to one of these two variables will also be related to the other variable and at a similar time lag. To overcome this problem, the relation between single-unit firing rate and Euclidian and equi-affine speeds was analyzed simultaneously and at multiple time lags using the following combined Euclidian/equi-affine speed multiple linear regression model:

$$f\left(t\right) = a + b\,\dot{s}\left(t+\tau_{\dot{s}}\right) + c\left|\dot{\sigma}\left(t+\tau_{|\dot{\sigma}|}\right)\right|.$$

where $f\left(t\right)$ is the unit's firing rate at time t, $\tau_{\dot{s}}$ and $\tau_{|\dot{\sigma}|}$ are the time lags for the Euclidian and equi-affine speeds, respectively, and a, b, and c are regression coefficients. Positive time lags correspond to the neural activity preceding the movement. The firing rates were computed for each spike train by convoluting it with a Gaussian kernel (SD = 50 ms). The influence of the Euclidian and equi-affine speeds was estimated using the measure of contribution (Stark et al. 2007)

$$C_{\dot{s}}\left(\tau_{\dot{s}}, \tau_{|\dot{\sigma}|}\right) = \beta_{\dot{s}}\left(\tau_{\dot{s}}, \tau_{|\dot{\sigma}|}\right)\rho_{\dot{s}}\left(\tau_{\dot{s}}\right),$$
$$C_{|\dot{\sigma}|}\left(\tau_{\dot{s}}, \tau_{|\dot{\sigma}|}\right) = \beta_{|\dot{\sigma}|}\left(\tau_{\dot{s}}, \tau_{|\dot{\sigma}|}\right)\rho_{|\dot{\sigma}|}\left(\tau_{|\dot{\sigma}|}\right).$$

Here, βs are the standardized regression coefficients for the corresponding parameters at time lag combinations $\left(\tau_{\dot{s}}, \tau_{|\dot{\sigma}|}\right)$, and $\rho\left(\tau\right)$s are the pairwise (Pearson) correlation coefficients between firing rate and the corresponding speed at time lag τ. At every time lag combination, the sum of the contributions equals the R^2 measure (Bring 1996). Therefore, the contribution of equi-affine speed can be interpreted as a fraction of the model R^2: the portion of speed-related firing-rate variance associated with equi-affine speed, taking into account Euclidian speed, at a given combination of time lags. The interpretation of the contribution for the Euclidian speed is analogous. Thus, we analyze contribution matrices whose two dimensions correspond to the time lags (from -0.3 to 0.3 s) of two movement parameters at which the values of contribution are computed.

Following Stark et al. (2007), a stripe (a horizontal or vertical set of values in a contribution matrix, all corresponding to the same time-lag of one of the two speed parameters) was deemed dominant if at least half of the constituent values were above $\max(R^2)/2$, where the maximum is taken over all R^2 values at all time-lag combinations of the two parameters. To determine the statistical significance

of movement relation at a given time lag combination (i.e., the significance of a given R^2 value), a permutation test was employed, in which firing rate profiles were randomly shuffled (1,000 times) relative to the movement parameters; the R^2s were recomputed, and the original R^2 value was compared to the shuffled values. That way, correlations between firing rate and movement parameters were abolished without altering the correlations among movement parameters, their auto-correlations, or the firing rate autocorrelations (Stark et al. 2007).

The values of the R^2 measure of how a linear model fits neural data on a sample-by-sample basis are of the order of 0.1 when a kinematic (position–velocity–acceleration) movement model is employed, presumably due to the Poisson-like noise of spiking neurons (Stark et al. 2007). To determine the range of the expected R^2 values when cells code Euclidean or equi-affine speed, firing rate profiles were generated using the following linear model:

$$f = a + b \cdot Speed,$$

where f is the firing rate, a and b are constants, and *Speed* is either Euclidian or equi-affine speed. Thus, f is deterministic given *Speed*. From f we generated Poisson spike trains by deciding at every millisecond whether a spike has been fired. That is, all the noise in the simulated spike trains originates solely from the Poisson spiking and not from an ill-fitting movement model. The resulting spike trains were then analyzed exactly like the real spike trains.

3 Results

3.1 A special role of parabolic drawing paths: mathematical considerations

We begin by merging the maximal smoothness optimality criterion and the geometric constraint formalized by the two-thirds power law. We therefore identify geometric paths for which the predictions of the constrained minimum-jerk model and the two-thirds power law coincide. The general necessary geometric condition for the paths that simultaneously satisfy the two principles, that is, imply identical predictions, is given by [for derivation, see Appendix A; a sufficient condition is also derived in Appendix A (Eq. (A11))]

$$x'''^2 + y'''^2 - 2x''x^{(4)} - 2y''y^{(4)} + 2x'x^{(5)} + 2y'y^{(5)} = \text{const},$$

where primes denote derivatives with respect to the equi-affine arc-length σ and numbers in brackets correspond to higher than third order derivatives w.r.t. σ. For a 6-times differentiable curve, differentiation of both sides of the above equality allows expression as the scalar product of the first and sixth order derivatives of the position vector with respect to σ:

$$\mathbf{r}'(\sigma) \cdot \mathbf{r}^{(6)}(\sigma) = 0. \tag{10}$$

This means that the first and the sixth order derivatives of paths complying with both models must be orthogonal to each other. Equation (10) needs to be solved simultaneously with Eq. (3) since Eq. (3) defines the equi-affine parameterization of the curve. Equation (10) is a general geometric expression that does not depend on time. In Appendix A (Eq. (A5)), we show how Eq. (10) can be expressed in terms of Euclidian and equi-affine curvatures without explicitly referring to the position coordinates along the path.

We have identified three kinds of geometric curves which simultaneously satisfy Eqs. (3) and (10): parabolas (Eq. (6)), circles (Eq. (A7)), and a special case of logarithmic spiral (Eq. (A8)).

Geometric movement primitives may underlie a more parsimonious (compact) representation of complex movements, especially because they are invariant under a group of geometric transformations. Mathematically, equi-affine invariance is advantageous since equi-affine transformations constitute the largest group of geometric transformations that conserve the velocity gain factor appearing in the two-thirds power law (Eq. (8)). Therefore, we seek the particular solutions of Eqs. (3) and (10) which are invariant under equi-affine transformations. As shown in Appendix B, only parabolas satisfy Eqs. (3) and (10) and are invariant under equi-affine geometric transformations. This implies that parabolic paths represent the *unique* geometric shapes in equi-affine geometry for which the trajectories that satisfy the two-thirds power law also satisfy the constrained minimum-jerk model (geometric transformations do not influence movement duration). We show in Appendix B that the mathematical generalization of Eq. (10) to the 3D case indicates that the unique 3D geometric path, invariant under 3D equi-affine transformations and providing maximal smoothness, is the parabolic screw (B13).

3.2 Parabolic patterns during drawing: evidence from monkey scribbling

Three data sets recorded from two monkeys were analyzed: (1) movements recorded at the beginning of the practice period of monkey O (17 consecutive sessions); (2) movements recorded at the beginning of the practice period of monkey U (16 consecutive sessions); and (3) movements recorded following a full year of practice by monkey U (17 consecutive sessions). Data sets (2) and (3) were analyzed separately to distinguish between practice, during which we expected to observe modifications in behavior, and well-trained behavior, during which we expected to observe steady-state behavior. Data with well-trained behavior of monkey O were not available.

The lengths of the recorded movement strokes, which were fitted with parabolic strokes, increased during practice (Fig. 2a, b). The per-session error of this fit was <0.006 for both monkeys (Fig. 2c). Considering strokes from all sessions together, the error of the fit was $D = 1.97 \times 10^{-3}$ (median; 95% confidence interval: [1.96 1.98] $\times 10^{-3}$). For both monkeys, the Euclidian (Fig. 2a) and equi-affine (Fig. 2b) lengths of the fitted parabolic strokes increased during practice, improving the representation of these movements by sequences of parabolic strokes. Columns 1 and 2 of Fig. 2 correspond to the beginning of practice of monkeys O and U, respectively, while column 3 corresponds to well-trained behavior of monkey U. An increase of the Euclidian and equi-affine lengths of the movement parts fitted with parabolic strokes is expected only in columns 1 and 2 (Fig. 2a, b, respectively). As column 3 shows, the lengths corresponding to the well-trained behavior of monkey U were greater than the lengths corresponding to the monkey's practice movements (column 2). Thus, the fitted parabolic strokes became longer with practice.

Since it is unlikely that empirical trajectories precisely follow a curve defined by an analytical formula, "drawn parabolas" refer to parabola-like strokes. To measure the extent to which scribbling movements were composed of such strokes we analyzed changes in equi-affine curvature (Eq. (5)) which may reflect practice. Equi-affine curvature is an equi-affine invariant whose value is exactly zero for parabolas (Sect. 2). We found that for movements performed after a number of practice sessions, the distributions of the equi-affine curvature κ and its absolute values $|\kappa|$ were concentrated close to zero (Fig. 3a, b respectively). During the first 5–6 practice sessions of each monkey, the equi-affine curvature consistently decreased and then stabilized (Fig. 3c). This indicates that after practice, the equi-affine curvature became closer to zero and thus more parabolic.

We next assessed the properties of geometric forms other than parabolic strokes which may provide good fit to the scribbling data. In particular, Eq. (4) implies that any parabolic stroke can be approximated arbitrarily well by some elliptic stroke (with equi-affine curvature close to zero); when κ is constant, Eq. (4) can be rewritten as a homogeneous linear system of two first-order equations with constant coefficients. Its local solution depends continuously on the matrix of coefficients which has only one variable, κ. We fitted

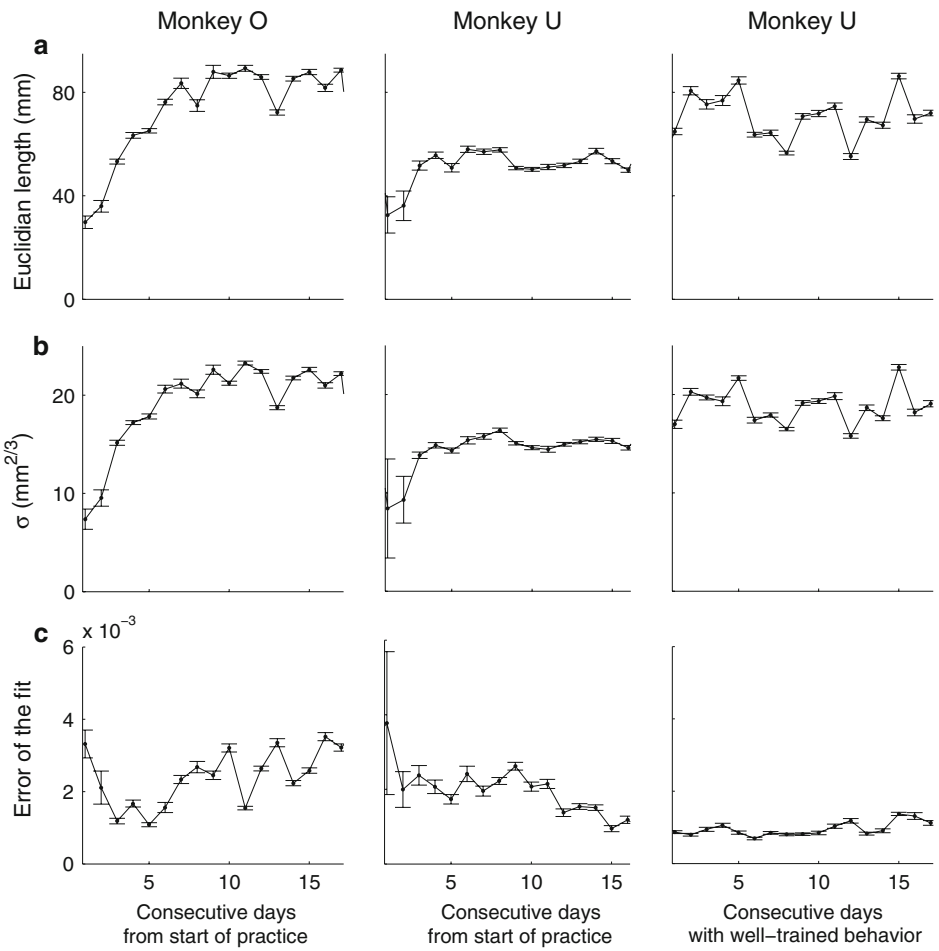

Fig. 2 Degree of fit and length of the parabolic strokes fitted to movement segments. **a** Euclidian lengths of the fitted parabolic strokes. Each plot shows median values (over sessions) and 95% confidence intervals; there were 50 sessions, with 3,144 strokes/session (median 95% range 2,816–3,796). **b** Equi-affine lengths of the fitted parabolic strokes. **c** Error of fit of parabolas fitted to path strokes between consecutive points of minimal Euclidian curvature (parameter D; see Sect. 2). Columns 1 and 2 correspond to the beginning of practice of monkeys O and U, respectively, column 3 corresponds to well-trained behavior of monkey U. See Results for more details

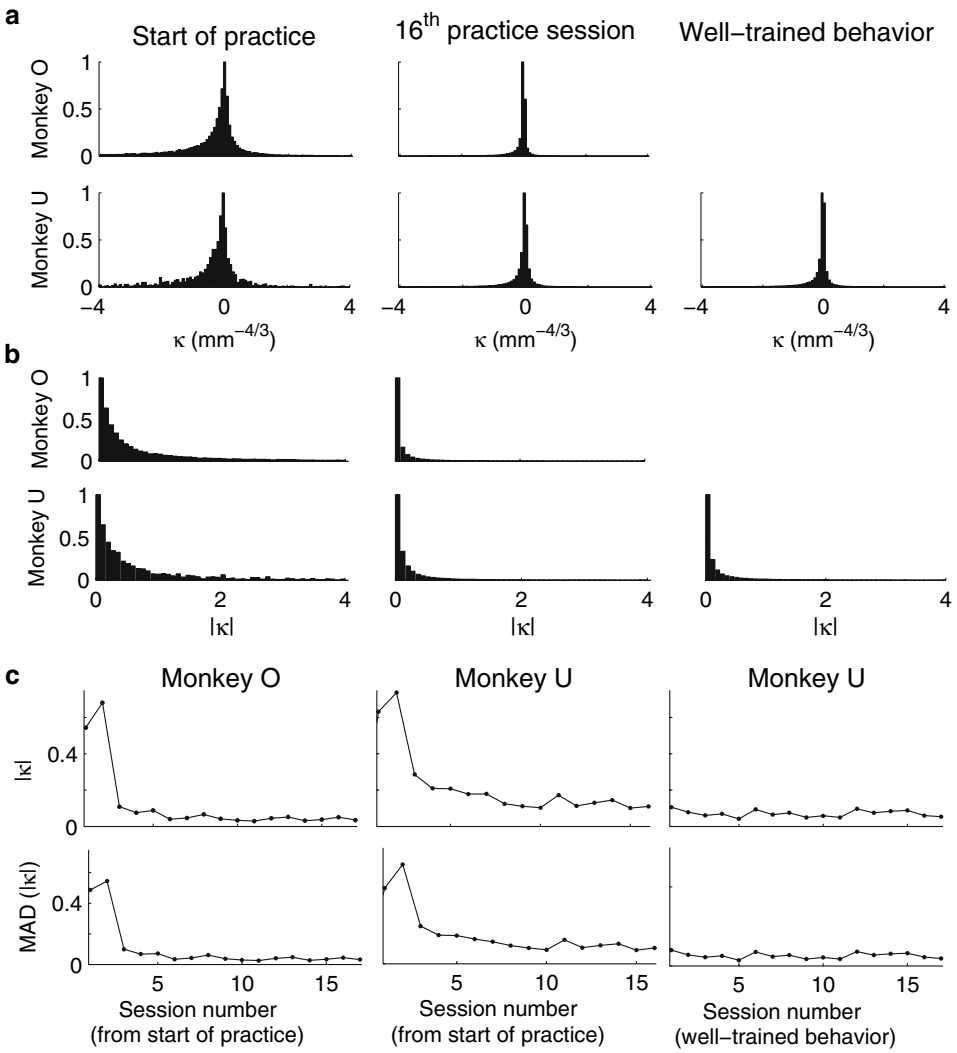

Fig. 3 Equi-affine curvature and its change after practice. **a** Distributions of equi-affine curvature for the first recorded session, a session after 15 practice days, and a session with well-trained behavior. Sampling rate is 100 Hz and sample sizes are, according to the practicing order: 28,259, 159,280 (monkey O); 1,445, 70,923, 202,471 (monkey U). Ordinate is measured in arbitrary units. **b** Distributions of the magnitude of the equi-affine curvature (data as in **a**). **c** *Upper row* median values of the magnitude of the equi-affine curvature. *Lower row* median absolute deviation of the magnitude of the equi-affine curvature, MAD = median(| |k| − median(|k|) |). After practice the equi-affine curvature became closer to zero and its distribution near zero became sharper

ellipses, polynomials of third, fourth, and fifth order parameterized by y in the canonical coordinate system and superimposed triplets of point-to-point movements (which fit parabolic paths well, Polyakov 2006, p. 149) to the movement parts to which parabolic strokes were fitted (Sect. 2). The R^2-based scores of deviation from the fitted path for the elliptic strokes were indeed smaller than the corresponding scores for parabolic strokes (Table 1, 1st and 2nd rows), but the difference in the deviation from the fitted path for parabolic models was of the order of 10^{-3} (compared with the maximum possible error $D = 1$, obtained when $R^2 = 0$). The values of the equi-affine curvature for the fitted ellipses were close to zero and for well-practiced movements these values were similar to the sample-wise estimates of $|\kappa|$ (cf. Fig. 3c).

Two considerations suggest that parabolic rather than elliptic strokes provide a better model for drawing movements. First, parabolas are defined by only four independent parameters while ellipses require five. Second, the distributions of κ peak at zero (histograms in Fig. 3a) with both negative and positive values. This indicates that the drawn trajectories are not elliptic, because for ellipses κ is strictly positive.

The fit with polynomials was also superior to the fit with parabolic strokes (Table 1, 3rd row). However, third, fourth, and fifth order polynomials are defined by five, six, and seven parameters, respectively (number of parameters in the polynomial expression plus one parameter for the orientation of the canonical system). The polynomials explained less than 1% of the data variance in addition to that already explained by the parabolic model. Finally, triplets of superimposed point-to-point movements provide a good fit to path elements fitted with parabolic strokes in our data, but again explained less than 1% additional data variance (Table 1, 4th row). However, on a geometric level, a triplet of linear paths is defined by at least seven parameters, three for the first path and two (orientation and relative position) for each of the other two paths.

Table 1 Results of fitting the same path elements with different types of curves

Curve			Number of parameters (including rotation)	Equi-affine geodesic	D (error of fit)		SIC score	
					Median	95% range	Median	95% range
1	Parabolas		4	Yes	1.97×10^{-3}	2×10^{-5}	−30.4	1.26×10^{-5}
2	Ellipses		5	No	8.32×10^{-5}	2.5×10^{-6}	−32.05	1×10^{-5}
3	Polynomials of order	3	5	No	3.49×10^{-4}	7×10^{-6}	−32.04	1.3×10^{-5}
		4	6	No	4.24×10^{-5}	6×10^{-7}	−33.67	3×10^{-7}
		5	7	No	1.21×10^{-5}	5×10^{-7}	−35.3	3×10^{-7}
4	Triplets of superimposed point-to-point movements		At least 7	No	1.52×10^{-3}	4×10^{-5}	−34.24	5×10^{-4}

Sample size is 50 sessions, with 3,144 strokes/session (median; 95% range: 2,816–3,796). The error of fit D for all curve types is similar, with differences of the order of 10^{-3}. An analysis of the trade-off between goodness-of-fit and model simplicity (number of model parameters) shows that the parabolic model corresponds to the highest value of the SIC score among all the models considered here. See Sect. 2 for details

To quantify the trade-off between goodness-of-fit and model simplicity (number of parameters), we employed the SIC score (Sect. 2). As the last two columns of Table 1 show, of all models considered here, the parabolic model yielded the highest SIC score (Kruskal–Wallis test, corrected for multiple comparisons, $P << 0.0001$). This indicates that the parabolic model is optimal in the sense of goodness-of-fit/simplicity tradeoff and therefore suggests that parabolas are more attractive candidates for simplifying movement representation and movement primitives.

One example specifically illustrates equi-affine invariant variables and parabolic paths in scribbling movements. Figure 4 shows a trajectory containing a part with equi-affine curvature below the median value during practice sessions ($|\kappa| < 0.1\,\mathrm{mm}^{-4/3}$; Fig. 3c) and is thus well approximated by parabolic strokes. The values of the equi-affine curvature and equi-affine velocity are shown in Fig. 4a. The corresponding low equi-affine curvature part (Fig. 4b) was well fitted with two parabolic strokes, with $D = 0.016$ for the first parabola and $D = 0.004$ for the second (Fig. 4c). This demonstrates that equi-affine curvature oscillating near zero indeed corresponds to parabola-like movement elements.

What is the origin of the abrupt deviation of the equi-affine curvature from zero (Fig. 4a)? The beginning and end of the movement in Fig. 4 correspond to very slow motion near an inflection point of the drawn path (a point at which Euclidian curvature is zero, equi-affine velocity is zero and equi-affine curvature is not defined). These are not fitted with parabolas. During slow motion, the quantization noise of the manipulandum (8,000 ticks per revolution) is relatively large, and any computation based on higher-order derivatives of position data is noisy. Therefore we did not use trajectory sections with slow motion in the equi-affine analysis (Sect. 2). Also, inflection points are degenerate in equi-affine geometry because equi-affine curvature is not defined for such points. Sharp changes in the values of the numerically derived estimates of equi-affine curvature, as observed near the segment boundaries in Fig. 4a, are characteristic of either slow motions or of movements near inflection points. The framework of equi-affine geometry is inappropriate for straight movements and for intervals near inflection points of curved movements.

Next, we addressed the possibility that the observed piecewise parabolicity of monkey trajectories can be explained solely on the basis of the increased smoothness of the movements following practice. An example of monkey drawing and the corresponding simulated maximally-smooth trajectory (Sect. 2) is shown in Fig. 4c. This example shows that the parabolic structure based on the values of Euclidian curvature c (minimum–maximum–minimum) is indeed more pronounced for the actual than for the simulated trajectory. Pooling movement elements from all the recording sessions, the values of the characteristic $\max(|c|) - \min(|c|)$ of the parabolic (rather than circular) structure (estimated for each path element fitted with parabolic stroke) were: for actual path strokes, $0.0804\,\mathrm{mm}^{-1}$ (median; 95% interval: 0.0796–0.0811) and for simulated strokes, $0.0411\,\mathrm{mm}^{-1}$ (median; 95% interval: 0.0408–0.0415). These characteristic values are higher for the recorded movements than for the simulated ones (Mann–Whitney U test, $P = 0.005$). Thus the convergence to piecewise parabolic scribbling patterns is not a trivial outcome of the increased smoothness of practiced movements.

3.3 Central representation of equi-affine speed: neurophysiological evidence

The special role of parabolas in equi-affine geometry and the analysis of monkey scribbling movements support parabolas as candidates for movement primitives. Using recordings

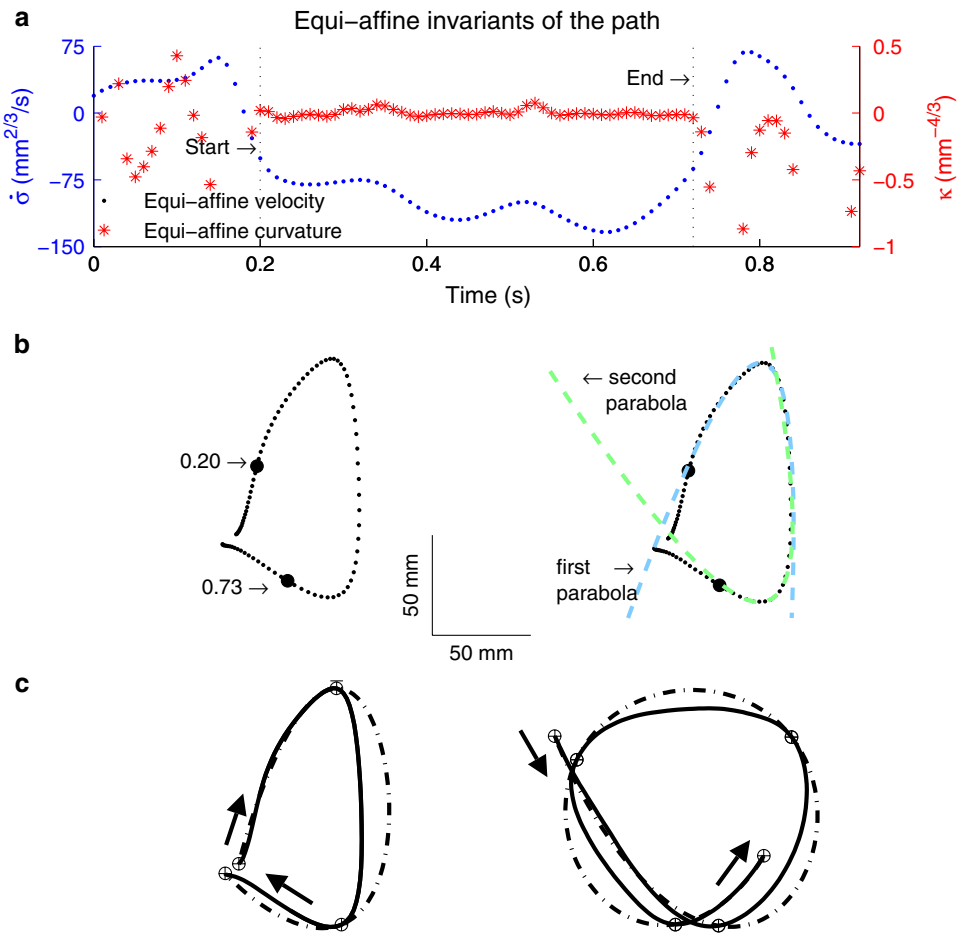

Fig. 4 Parabolic nature of drawing. **a** Equi-affine velocity (*dots*) and curvature (*asterisks*) for a scribbling segment. The position data are sampled at 100 Hz. The equi-affine curvature is nearly zero between 0.20 and 0.73 s. **b** The actual drawing made by the monkey. Since parabolas are characterized by zero equi-affine curvature, the motion segment can be well-fitted by parabolas (*dashed lines*). **c**. The movement trajectory (*continuous line*) and the simulated minimum-jerk trajectory (*dot-dashed line*; Sect. 2), for two movement segments (*left* drawn by monkey O, same as in **b**; *right* drawn by monkey U). The minimum-jerk trajectory passes through several via-points which form vertices of parabolic segments. In the left/right segments, the two/four via-points correspond to two/four fitted parabolas. The differences between the maximal and minimal Euclidian curvatures ($\max(|c|) - \min(|c|)$) for path strokes fitted with parabolas are larger for the actual versus the simulated movements (Sect. 3)

from macaque motor cortex during well-trained scribbling, we test directly whether equi-affine speed is represented in motor cortical activity and then examine whether composing movements by concatenating parabolic strokes (primitives) may have a central origin.

The activity of 87 well-isolated units recorded during the scribbling task was analyzed. The activity of 72 units (83%) was related to the monkey's hand position, velocity, acceleration, or some combination of these kinematic variables (units were analyzed as described in Stark et al. 2007). The contribution matrices for the combined speed model (Sect. 2) for one of these units are shown in Fig. 5a. The R^2 for this unit was 0.094, indicating that 9.4% of the firing rate variance was accounted for by Euclidian speed $\dot{s}$ and/or equi-affine speed $|\dot{\sigma}|$.

Because the R^2 value here may seem low, we investigated the R^2s obtained from a simulated neuron that spiked according to a time-varying Poisson process modulated solely and exactly by equi-affine speed (Sect. 2). The median R^2 for the simulated spike trains was 0.081 (95% confidence interval over 1,000 simulations: [0.079 0.083]), similar to the results from the neural data (median R^2 over 16 speed-related (see below) cells: 0.08; Mann–Whitney U test: $P = 0.65$). Thus, low R^2s are expected from motor cortical neurons firing in a Poisson-like manner according to equi-affine speed and analyzed on a sample-to-sample basis.

For the unit depicted in Fig. 5a, the firing rate is movement-related because contribution of equi-affine speed to the firing rate variance is dominant as the right matrix contains a vertical dominant stripe (see Sect. 2 for definition of a dominant stripe) at a time lag of 0.12 s, indicating that neural activity precedes movement (permutation test, $P < 0.05$). In contrast, the contribution matrix for the Euclidean speed (left) does not contain a dominant stripe.

The results of Poissonian simulation and the permutation test show that the combined Euclidean/equi-affine speed model provided a good fit for the firing rates of 16/72 (22%) of the movement-related units (permutation test, $P < 0.05$; Fig. 5b). The activity of seven of these units (44%) was related to both Euclidean and equi-affine speeds. However, equi-affine speed was dominant in the activity of six units (38%) whereas Euclidian speed was dominant for only three

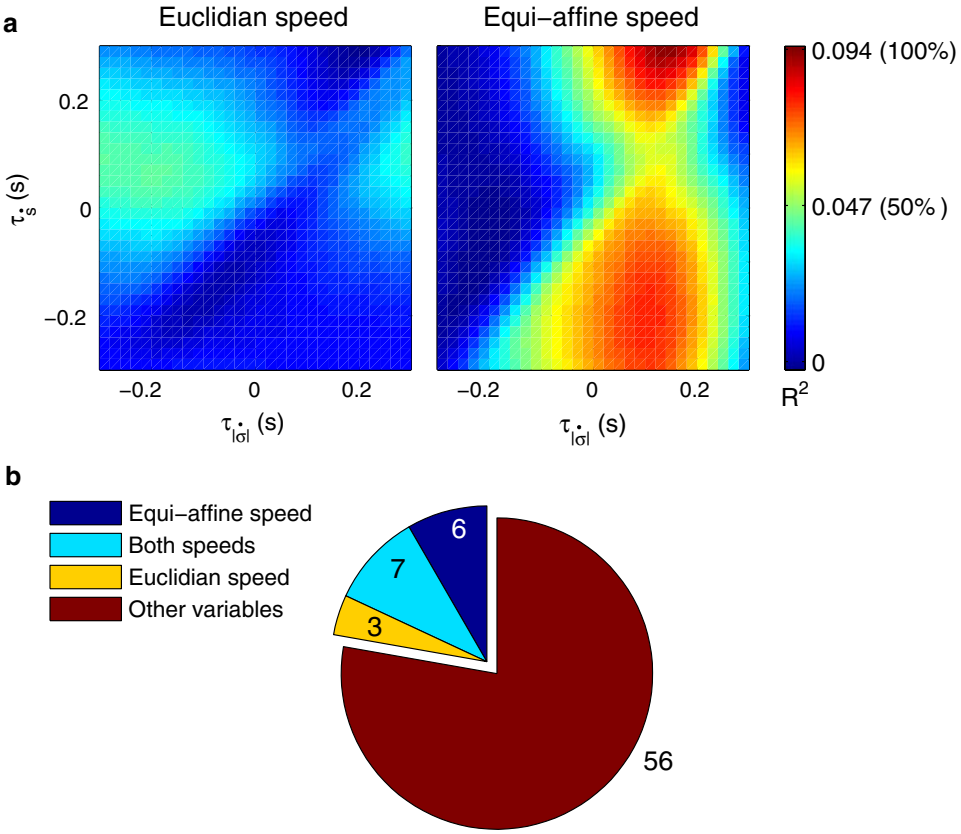

Fig. 5 Motor cortical activity related to equi-affine speed. **a** Contribution matrices used to compare the representation strength of Euclidian (*left*) and equi-affine (*right*) speeds in the activity of one motor cortical unit. Contributions are shown as fractions of the total R^2 (0.094 in this case) of a linear model including both speeds (Sect. 2). The vertical stripe in the right matrix indicates that the equi-affine speed is more strongly represented. The stripe appears at a time lag of 0.12 s, where neural activity precedes the movement. **b** Number of movement-related units whose activities receive dominant contribution from the equi-affine and/or Euclidian speeds

units (19%). Thus, although only a few units were modulated exclusively by speed, more of these were related to equi-affine than to Euclidian speed.

3.4 Neurophysiological evidence for a central representation of parabolic drawing components

If unique states of ensemble activity of motor cortical cells represent movement primitives, it should be possible to associate such states with distinct movements having common characteristics. To test this, we used hidden Markov modeling (HMM; Abeles et al. 1995; Gat et al. 1997) and segmented motor cortical activity in an unsupervised manner, without using any information about the concurrent movements. The idea behind using an HMM is that the nervous system may dynamically change its internal state with time. Such states may be unobservable (hidden) but expressed in the activity of the recorded neurons. The aim of the HMM analysis is to reveal the probability structure of the postulated underlying Markov process and its neuronal expression and, thus, assign a probability to each state at every instant. Neural activity can subsequently be segmented according to the transitions between dominant states.

We required a data segment with a dominant state to have probability above 0.5 for at least 0.1 s with its time-average at least 0.75. One such segmentation is demonstrated in Fig. 6, showing a sequence of observations consisting of vectors of spike counts (Fig. 6a). The model provides the a posteriori probabilities of the states as a function of time (Fig. 6b shows a period when state 1 was dominant). The periods identified with states 2, 4, 5, 6 are either too short or have time-averaged probability below 0.75 and therefore are not dominant. While segmentation was unsupervised, some states corresponded to parabola-like movement elements (Fig. 6c).

The HMM analysis was applied to the activity of a group of simultaneously recorded motor cortical units (5–12 units/session, 8 sessions). For one session, the relationship between the results of the HMM-based segmentation and the piecewise parabolic structure of the drawing movements was especially pronounced: a graphical sketch of the transition probabilities between the states is shown in the central part of Fig. 7a (HMM was learned for eight states in this session). Movement periods associated with periods of dominance for each of the eight states were lagged relative to the neural activity by 0.14 s. A single time lag was used, although many units were active during each state and different neurons can have diverse time lags (Moran and Schwartz 1999; Stark et al. 2007). The specific time lag of 0.14 s provided the highest similarity between shapes associated with each state. The paths identified with each state are also depicted in Fig. 7a. These drawings correspond to the periods when states were dominant as defined above. Nearly 50% of duration of the

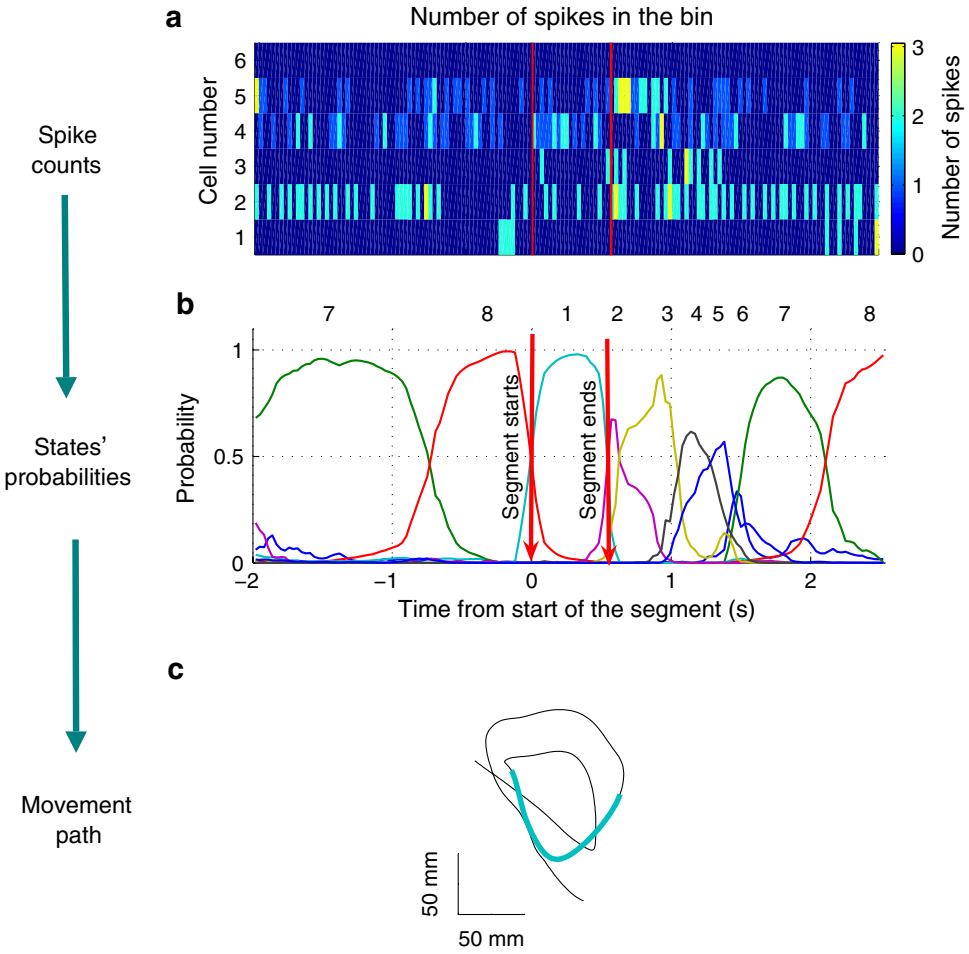

Fig. 6 Illustration of movement segmentation according to a hidden Markov model (HMM). **a** The input is a time series of observations, quantified as vectors of spike counts in non-overlapping time bins of 30 ms. **b** The HMM model, learned here for eight states, provides a posteriori probabilities as temporal functions. The neural activity can then be segmented based on the dominant probabilities. The numbers above the plot correspond to the state with the highest instantaneous probability. **c** The movement corresponding to the segment based on state 1 is *highlighted*; this segment is parabolic

neural data analyzed in this session was identified with the periods of dominant a posteriori probabilities of the hidden states.

States 1–4 corresponded to faster movements (Fig. 7b), which formed geometric shapes easily identifiable as parabolic strokes with specific orientations (Fig. 7a). State 1, for example, corresponded to parabolic strokes oriented around 270 degrees (direction of the normal at vertex). States 1 and 2 could be identified with single parabolic strokes, whereas states 3 and 4 corresponded to elements from sequences composed of two parabolic strokes. States 5–8 corresponded to slower movements, presumably associated with periods of rest. Thus, the HMM segmentation, although unsupervised, resulted in partitioning movement into sets of parabola-like elements.

3.5 Obstacle avoidance movements passing through a single via-point are parabola-like

We now re-examine the geometric properties of 2D trajectories which fit well with human planar obstacle avoidance and via-point movements. Such movements start and end at rest and are constrained to avoid an obstacle or pass through an a priori specified single via-point. They can be described by the original minimum-jerk model (Hogan 1984; Flash and Hogan 1985). In this model, and in contrast to the constrained minimum-jerk model, hand path is not specified a priori. The x and y coordinates of the trajectories predicted by the original minimum-jerk model are described by fifth order polynomials in time (Flash and Hogan 1985; see Sect. 2 for a distinction between movement path and trajectory). Thus, hand acceleration generally is not constant, and the integrated jerk is not zero. Nevertheless, such minimum-jerk trajectories can be well approximated by parabolic paths. Figure 8 shows two examples of trajectories starting at the point (0, 0), going through a via-point, and ending at (1, 0), and the parabolas that match their paths. The fit was very good for the parabolic model (Fig. 8a: $D = 6.5 \times 10^{-5}$; Fig. 8b: $D = 5 \times 10^{-5}$). The fit was good for all tested via-point locations ($x \in [-2.5\ 2.5]$, $y \in [-1.5\ 1.5]$), with $D < 0.001$. Thus, movements going through a single via-point are parabola-like, suggesting that obstacle avoidance movements are also parabola-like.

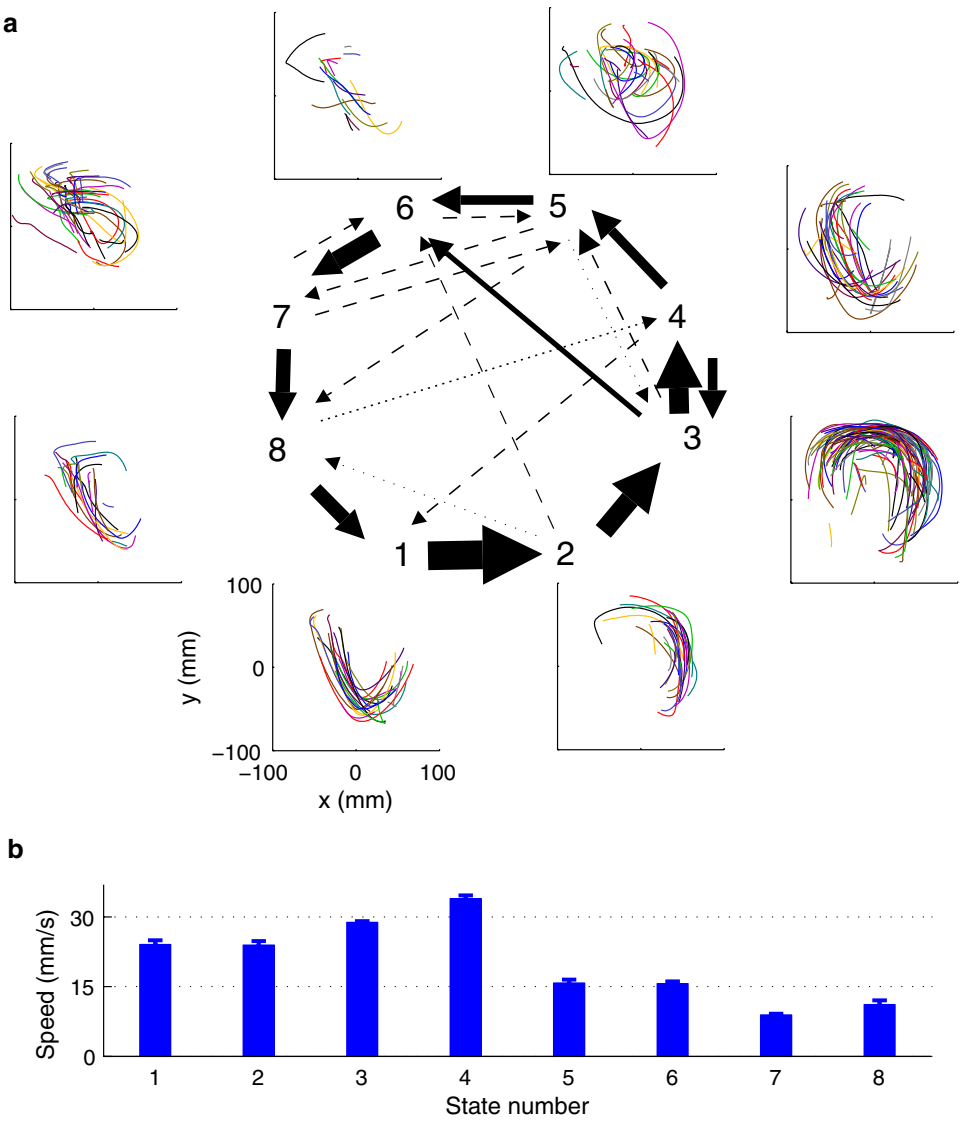

Fig. 7 Example of HMM results for one session. **a** *Center* Transition probabilities between states. The *thickest arrows* correspond to the highest probabilities, and the *dashed and dotted arrows* correspond to gradually lower probabilities. The largest depicted probability is ∼15 times higher than the lowest. *Periphery* paths corresponding to the states (for presentation purposes, the paths with shortest and longest durations within each state were omitted so only 90% of the paths are shown). **b** State-wise medians for the speeds, estimated across all samples of the segments identified within each state. *Error bars* show 95% confidence intervals. Movements corresponding to the parabolic states (1–4) are fast, whereas movements identified with other states correspond to periods of rest

3.6 Parsimonious geometric representation of trajectories by sequences of parabolic strokes

Movement primitives were proposed to solve the problem of parsimonious representation of continuous complex movements (Flash and Hochner 2005). Here, we propose a mechanism for generating complex piecewise parabolic trajectories. All parabolic paths have zero equi-affine curvature at every location along the path. We therefore conclude from the main theorem (Sect. 2) that any two parabolic strokes can be aligned with each other using some equi-affine transformation, whenever the equi-affine arc-lengths of these two strokes are equal. Consequently, parabolic elements offer a compact representation of hand trajectories because *any* parabolic stroke can be transformed into another using a unique equi-affine transformation and a uniform spatial scaling (both defining a unique affine transformation). To examine this suggestion, consider a geometric description of a movement that is involved in drawing a parabolic stroke with a prescribed duration and call this a "movement template". Given the template's trajectory, only six constants ($\alpha, \beta, \gamma, \delta, a, b$ in Eq. (1)) are required for a full geometric description of the new parabolic stroke. This implies that different parabolic elements composing piecewise parabolic drawings can be generated from a single parabolic template.

Figure 9 illustrates generation of complex movements using equi-affine transformations of a single parabolic template. The parabolic strokes in Fig. 9a result from mathematical simulation. They can be concatenated into a composite pattern. A similar principle can be seen in the scribbling movements in Fig. 9b–d, where only three strokes were needed to fit the drawing movement, and the fitted parabolic strokes were long (mean lengths in Fig. 9b–d: 92, 110, and 110 mm, respectively). Moreover, the fitted parabolas often overlapped (Figs. 4c, 9b–d), suggesting the existence of smooth transitions from one parabola to the next.

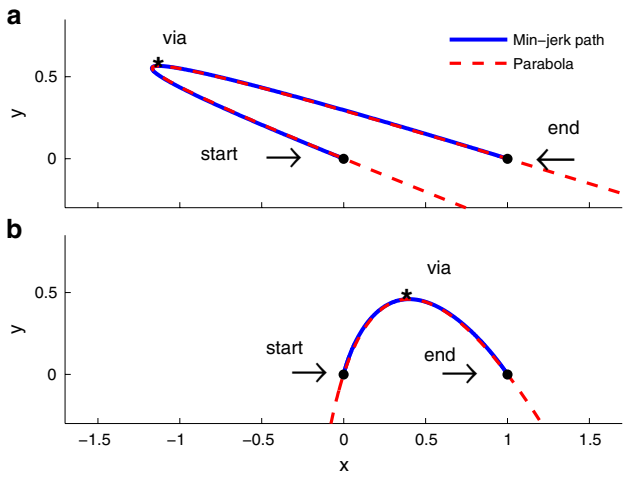

Fig. 8 Minimum-jerk trajectories and fitted parabolas. Two trajectories predicted by the minimum-jerk model with one via-point (not several via-points and not the constrained minimum-jerk model), starting at (0, 0) and ending at (1, 0). For the parabolic model, $D = 6.5 \times 10^{-5}$ (**a**) and 5×10^{-5} (**b**). These examples illustrate that minimum-jerk trajectories with one via-point follow nearly parabolic paths. Very good degrees of fit were obtained for a large range of via-points (Sect. 3)

4 Discussion

We have derived a mathematical equation for a common geometric template of two models, the two-thirds power law and the constrained minimum-jerk model. We prove that parabolic strokes constitute a unique solution which is invariant under equi-affine transformations. Although both models are merely kinematic approximations, we found empirical support for their common geometric invariant feature, parabolas. Further, we found evidence for a statewise representation of drawing movements in motor cortex in which some states were identified with clusters of parabolic strokes. Finally, we provided corroborative evidence that a non-Euclidian, equi-affine metric is relevant for the neural representation of hand trajectories.

We therefore propose that the motor control system constructs well-practiced spontaneous planar scribbling movements by stringing together several geometrically invariant primitives—parabolic strokes. An important implication of fitting parabolic strokes to the recorded movements is the resultant dimensionality reduction: a large variety of different parabolic strokes can be generated by applying sequences of affine transformations to a single parabolic element (Fig. 9). Hence, parabolic strokes are optimal with respect to motion planning and production in their smoothness and parsimonious representation.

The term "parabolic primitive", used throughout, indicates any parabola-like shape which can be fitted by many different kinds of curves that approximate parabolas arbitrarily well. Among these are ellipses and hyperbolas with near-zero equi-affine curvature and higher order polynomials describing x and y coordinates. However, several considerations suggest that parabolas are preferable candidates. First, the simplest parabola-like shapes are parabolas, these being defined by only four independent parameters, while ellipses and hyperbolas require five and polynomials of order n in plane require $n + 2$ parameters ($n + 1$ describing polynomial parameterization and 1 describing rotation), Table 1, 3rd column. Second, the distribution of the equi-affine curvature of drawing movements peaked near zero whereas ellipses/hyperbolas have strictly positive/negative equi-affine curvature (Fig. 3a). Third, the equi-affine curvature became smaller during practice and the fitted parabolic strokes became longer (Fig. 3c). Finally, parabolas have the highest SIC score among all shapes under consideration (Table 1).

4.1 Movement primitives and equi-affine geometry

Earlier studies suggested movement primitives which provide a compact description of movement at different levels of the motor hierarchy. The existence of motor primitives was demonstrated at the level of forces generated by muscles operating on the limbs (Bizzi et al. 1991; Giszter et al. 1993; Nichols 1994; Kargo and Giszter 2000; Mussa-Ivaldi and Bizzi 2000; Mussa-Ivaldi and Solla 2004), at the level of muscle synergies (Tresch et al. 1999; d'Avella et al. 2003; Hart and Giszter 2004; Ivanenko et al. 2004, 2005; d'Avella and Bizzi 2005; d'Avella et al. 2006), at the level of motion kinematics (Morasso and Mussa-Ivaldi 1982; Flash and Henis 1991; Burdet and Milner 1998; Krebs et al. 1999; Sanger 2000; Rohrer and Hogan 2003; Fishbach et al. 2005; Rohrer and Hogan 2006), and at the level of units of computation in the sensorimotor system (van Zuylen et al. 1988; Thoroughman and Shadmehr 2000).

Our general proposition is that hand movements satisfy the two-thirds power law and the minimum-jerk model because they are piecewise parabolic and their representation is based to some extent on equi-affine invariance. That is, geometric properties of movements and the tendency to keep the equi-affine speed close to constant are consistent with observed movement kinematics, namely the two-thirds power law and the tendency of the trajectories to minimize jerk. Parabolas are the simplest non-straight shapes (in terms of a Taylor expansion), and we propose that non-straight geometric movement primitives are used to parsimoniously represent curved movements. First, natural movements are both straight and curved, the latter quite often showing equi-affine invariance while straight lines have zero equi-affine length. Second, the use of straight lines as a basis for the representation of parabolic strokes requires additional parameters (Table 1, 4th row).

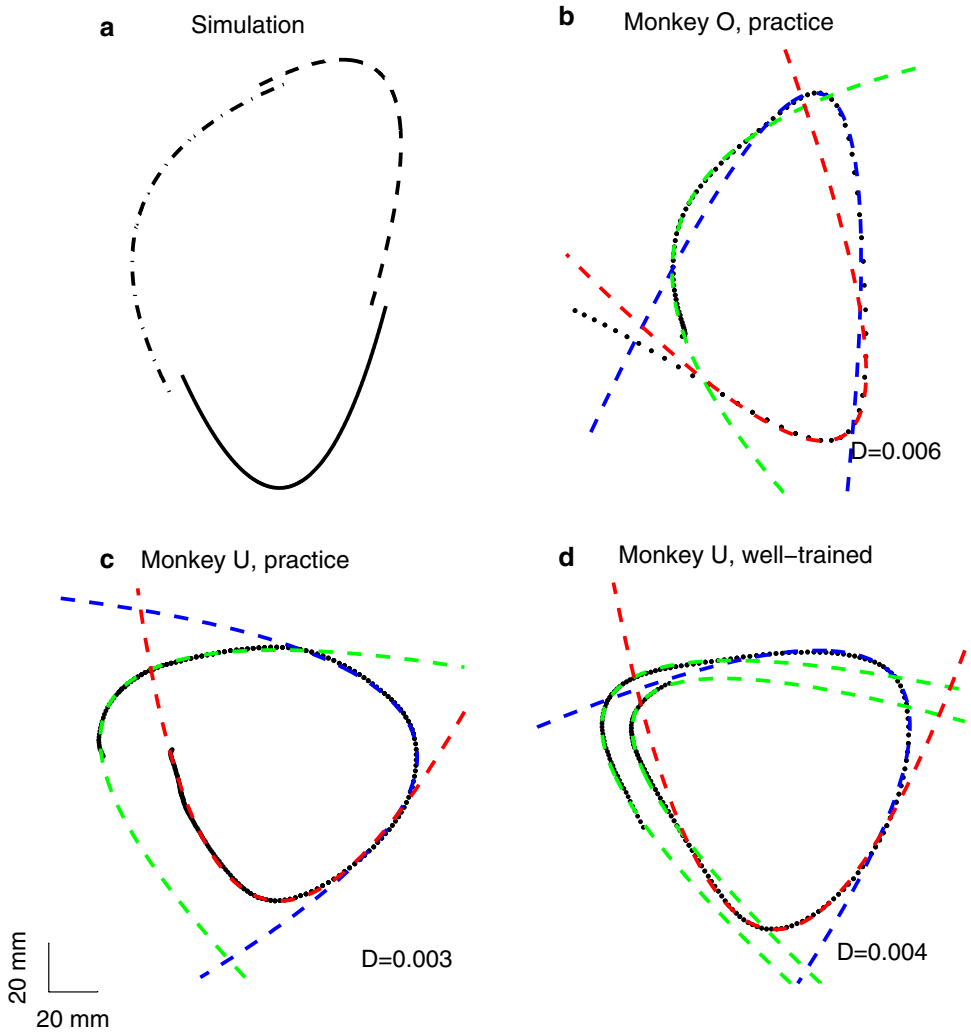

Fig. 9 Concatenation of parabolic movement segments generated from the same parabolic template. **a** Simulation of three parabolic elements, obtained from the same parabolic stroke by applying to it different equi-affine transformations. **b–d**. Examples of monkey drawing movements from different practice periods, and the parabolic strokes fitted to them. The median error of the parabolic fits is shown in each panel

Vector summation, used previously to combine movement primitives (e.g., Bizzi et al. 1991; Kargo and Giszter 2000), is neither defined for elements of a sequence, nor for parabolic elements. Instead, we propose that movements are produced by concatenating modifiable geometric shapes acted upon by sequences of geometric transformations from the equi-affine group. However, this principle is general and may be applied to other geometric primitives (e.g., corresponding to other non-Euclidean transformations), to be examined in the future.

Moving with a constant acceleration along a single parabolic stroke obeys the two-thirds power law (Appendix C). However, drawing each separate parabolic component within a sequence at a constant acceleration (to satisfy the two-thirds power law) would give rise to abrupt changes in acceleration and high jerk values at the transitions between adjacent parabolas. Therefore, only the common geometric (and not temporal) predictions of the minimum-jerk model and the two-thirds power law, namely, that movements consist of sequences of parabolic segments, were substantiated by the recorded drawings. For trajectories composed of more than one parabola, the predicted speed along each parabolic component deviates somewhat from the speed predicted for that component if executed alone. Consistent with this is our observation that the convergence towards parabola-like drawing sequences during practice did not improve the fit of the monkey scribbling movements to the two-thirds power law or to the minimum-jerk model (Polyakov 2006, pp. 215–219). Consequently, smoothing may be applied by the motor system at the transitions between neighboring elements and thus the geometric levels of planning may precede the temporal level (see also Torres and Andersen 2006; Biess et al. 2007).

4.2 Why equi-affine invariance

Previous studies suggested that the equi-affine invariant two-thirds power law is simply a by-product of peripheral biomechanical factors such as low-pass properties of muscles

(Gribble and Ostry 1996) or the effects of non-linear forward kinematic transformations (Sternad and Schaal 1999; Schaal and Sternad 2001; Dounskaia 2007). Our behavioral data are limited to the end-effector trajectories, and therefore we did not study the potential contribution of limb biomechanics to the piecewise parabolicity of movements. However, a central origin of the two-thirds power law was previously demonstrated using neural population vectors (Schwartz 1994). Here we showed that equi-affine geometric invariance (preserving the two-thirds power law) is represented in the activity of single motor cortical neurons (Fig. 5). Moreover, the representation of objects and geometric forms in the human visual system may possess properties of affine invariance (Pollick and Sapiro 1997; Todd et al. 2001). In particular, common affine representation of motor production and visual perception may simplify the drawing of similar shapes independent of the relative orientation of the eye and drawing plane. Indeed, movements obeying the two-thirds power law are perceived as being more uniform (Viviani and Stucchi 1992; Levit-Binnun et al. 2006). In a recent fMRI study Dayan et al. (2007) demonstrated that brain areas related to motor production, visual motion processing, and action observation reflected compliance with the two-thirds power law during motion perception. Thus, the local relationship between motion velocity and curvature may reflect complementary central and peripheral mechanisms (Ivanenko et al. 2002).

The formation of smooth, parabola-like drawing shapes may be based on a smooth equi-affine invariant interpolation between initial and final movement directions (Handzel and Flash 2001; Flash and Handzel 2007). Among all interpolating curves, parabolas are equi-affine geodesics maximizing equi-affine distance (Sect. 2). Hence, the generation of parabolas may increase movement duration (assuming equi-affine speed is kept constant), leading to smaller jerk in a tradeoff between movement duration and smoothness. Apparently, the representation of a complex planar curve as a sequence of points and tangents at those points leads to an affine-invariant model of parabolic polygons composing the curve (Craizer et al. 2007). An earlier indication that parabolas may serve as geometric movement primitives during drawing movements was provided by Polyakov (2001).

We propose that when drawing or producing a path, the biological system relies on pre-existing representations, even when the path is not fully pre-represented. Instead, the movements being generated are constructed from geometrical representations of simpler templates stored in memory. This mode may be implemented using piecewise parabolicity and allows a more parsimonious representation of hand trajectories (see above). Maximization of both smoothness and parsimony may be important for motor control, and both can be satisfied simultaneously by planning motion in terms of parabolic primitives.

4.3 Mathematical generalization to 3D movements

Our theoretically-derived candidate 3D geometric primitive is a spatial cubic parabola (B13). However, greater smoothness and parsimony is expected for planar trajectories constructed from planar parabolas than for 3D trajectories (Appendix B). Soechting and Terzuolo (1987a) claimed that human subjects are incapable of producing true 3D arm movements and that their 3D movements are composed of piecewise planar segments (Soechting and Terzuolo 1987b). In contrast, others have reported that 3D hand movements are not piecewise planar (Maoz 2007; Pollick et al. 2008). Hence, future experimental studies are needed to examine whether natural 3D movements can be decomposed into planar parabolic strokes which are connected by segments of cubic parabolas.

4.4 Statewise representation of movements in the motor cortex

We showed that different combinations of elementary movement segments correspond to different sequences of neuronal states (Fig. 7). Sequential behavior is encoded in the activity of motor cortical neurons (Carpenter et al. 1999; Hatsopoulos et al. 2003; Ben-Shaul et al. 2004), suggesting that the cortical control of movement may be partially discrete rather than involve only continuous parameters. In the gustatory cortex of rats, repeatable sequences of states of neural activity were interpreted as evidence that sensory neurons act as elements of a systems-level dynamic process (Jones et al. 2007). We propose that motor cortical neurons have a similar role in movement production.

Our results suggest that parabolic movements identified in monkey scribbling may, through the process of practice, form a behavioral output of dynamically-switching cortical "attractors". This is consistent with the motor system achieving more parsimonious control strategies after practice/learning. Convergence toward attractor-like neural activity during practice via Hebbian learning may underlie the superposition/co-articulation of sequences of point-to-point motion units into more compact and smoother parabola-like movement components. Supporting this possibility, Sosnik et al. (2004) showed that rehearsal of a sequence of elementary planar point-to-point movements by human subjects leads to the formation of more complex smooth geometric primitives. Moreover, the smooth human movements were well-fitted with minimum-jerk trajectories passing through a single via-point. Our results imply that acquired geometric primitives could be parabola-like elements. This shows how a minimum-jerk trajectory connecting two points of rest and passing through a single via-point may aid modeling a kinematic rule of parabolic motion.

A single parabolic drawing can be decomposed into three point-to-point movements, each with a bell-shaped speed profile. Each bell-shaped speed profile can, in turn, be decomposed into three smaller identical bell-shaped speed profiles, and so on (Polyakov 2006, pp. 150–151). However, a triplet of point-to-point movements is defined by at least seven parameters while a parabola is defined by only four parameters, thus providing more compact representation. We suggest that in the hierarchy of geometric primitives, point-to-point movements constitute the lowest level, whereas parabola-like shapes constitute the next level above and therefore are acquired during learning to achieve more efficient performance of complex movements (in terms of smoothness and representation complexity).

Averbeck et al. (2002, 2003) associated different movement sequences with distinct patterns of activities of prefrontal neuronal ensembles. Hatsopoulos et al. (2007) introduced the "pathlet", a temporally extensive and complex movement element encoded by a single motor cortical neuron. Kalman and particle filtering techniques (Wu et al. 2004; Brockwell et al. 2007) constitute state-space approaches to the reconstruction of hand movements, based on probabilistic models of spiking activity for given movement trajectories. However, the nature of movement primitives has not been previously studied by unsupervised segmentation of the neural population activity. We therefore studied the emergence of elementary building blocks in spontaneous movements (not constrained by any specific cue) and their representation in motor cortical activity. In view of the dynamic nature of movement coding by single motor cortical units (Sergio et al. 2005), segmenting the neural ensemble activity by HMM may allow analyzing the coding separately in each individual state. This may provide insights into neural function and improve its decoding, especially in closed-loop adaptive brain–computer interfaces.

In summary, parabolic primitives capture two different but related properties: equi-affine invariance, leading to the parsimony of movement representation, and trajectory smoothness. We have provided empirical support for the existence of parabolic movement elements, representation of equi-affine geometric invariance in motor cortex, and state-dependent representation of stereotypical movements. Future work will seek geometric paths for which other kinds of geometric invariance and optimality are simultaneously satisfied and analyze properties of motor cortical neurons (e.g., tuning) during different states of ensemble activity.

Acknowledgments We are grateful to Yoram Ben-Shaul and Zoltan Nadasdy for providing experimental data (monkeys O, U). We thank Jason Friedman for valuable comments on the manuscript, Ido Cohn, Jacob Goldberger, and Victor Kasatkin for their help with the HMM data analysis, Amir Handzel for providing us with the code for estimating the equi-affine parameters from samplewise data, Magnus Richardson whose work inspired an important part of the current research, and Edriss Titi, Daniel Bennequin, and Hector Sussmann for useful discussions. This research was partially supported by DIP (Deutsch-Israelische Projektkooperation), the Israeli Ministry of Science, and by the Israeli Science Foundation. Tamar Flash is an incumbent of the Dr. Hymie Moross Professorial Chair.

Appendix A: Paths for which the predictions of the two-thirds power law and the constrained minimum-jerk model coincide

We first derive an equation that must be satisfied by the paths for which the two-thirds power law and the constrained minimum-jerk model provide identical predictions — a necessary condition. We then derive a general sufficient condition on a path which implies that the path complies with both models.

As mentioned in the main text, motion according to the two-thirds power law along a movement segment for which the gain factor K is constant is equivalent to moving at a constant equi-affine velocity ($\dot{\sigma} = \text{const}$). Hence, we wish to find the paths along which motion according to the rule ($\dot{\sigma} = \text{const}$) minimizes the jerk cost compared to all other possible trajectories along those paths. Let us consider the *convex* (that is without inflection points) path ξ with equi-affine length Σ_ξ given by the vector function $\boldsymbol{\xi}(\sigma) = \{x(\sigma), y(\sigma)\}; \sigma \in \left[0, \Sigma_\xi\right]$ parameterized by the equi-affine arc-length. Let

$$J_\sigma(\xi) = \frac{1}{2}\int_0^T \left[\dddot{x}^2(\sigma(t)) + \dddot{y}^2(\sigma(t))\right] \mathrm{d}t$$

be the jerk cost along the path whose trajectory is defined by the functions $\boldsymbol{\xi}(\sigma)$ and a strictly increasing function $\sigma(t)$ such that $\sigma(0) = 0$, $\sigma(T) = \Sigma_\xi$ (for a strictly increasing function $\sigma(t)$, $\sigma(t_2) > \sigma(t_1)$ whenever $t_2 > t_1$, i.e., the graph of the function always increases; for example, for $\Sigma_\xi = 1$ and $T = 1$, the function $\sigma(t)$ could be $\sigma = t$ or $\sigma = t^2$). In general, the costs are different for different trajectories that follow the same path but with different expression for $\sigma(t)$.

Let $\sigma_\xi^*(t)$ be the solution of the minimization problem stated above:

$$\sigma_\xi^*(t) = \arg\min_{\sigma(t)} J_\sigma(\xi). \tag{A1}$$

Our goal is to find paths $\{\boldsymbol{\xi}\}$ for which the corresponding solutions of the minimization problem $\sigma_\xi^*(t)$ are linear functions of time (the equi-affine velocity is constant) or, equivalently, for which the motion minimizing jerk also satisfies the two-thirds power law model. Thus

$$A = \left\{\xi : \dot{\sigma}_\xi^*(t) = \text{const}\right\}. \tag{A2}$$

For the function $\sigma(t) \in [0, \Sigma_\xi]$ and its inverse function $t = \tau(\sigma) \in [0, T]$, we denote

$$v_a = v_a(\sigma) = \frac{\mathrm{d}}{\mathrm{d}t}\sigma(t)\Big|_{t=\tau(\sigma)}$$

$$w_a = w_a(\sigma) = \frac{\mathrm{d}^2}{\mathrm{d}t^2}\sigma(t)\Big|_{t=\tau(\sigma)} = v_a\frac{d}{d\sigma}v_a = v_a' v_a$$

$$j_a = j_a(\sigma) = \frac{d^3}{dt^3}\sigma(t)\Big|_{t=\tau(\sigma)} = w_a\frac{\mathrm{d}}{\mathrm{d}\sigma}w_a = v_a'' v_a^2 + v_a'^2 v_a$$

where a prime denotes differentiation w.r.t. σ (here we used the following property:
$\frac{\mathrm{d}}{\mathrm{d}t}f(\sigma(t)) = \dot{\sigma}\frac{\mathrm{d}}{\mathrm{d}\sigma}f(\sigma) = v_a f'$.
So, finally,

$$\begin{aligned} J_\sigma &= \frac{1}{2}\int_0^T \left(\dddot{x}^2 + \dddot{y}^2\right)dt = \frac{1}{2}\int_0^{\Sigma_\xi}\frac{1}{v_a}\left[\left(x'''^2 + y'''^2\right)v_a^6\right. \\ &\quad + 9\left(x''^2 + y''^2\right)w_a^2 v_a^2 + \left(x'^2 + y'^2\right)j_a^2 \\ &\quad + 6\left(x'''x'' + y'''y''\right)v_a^4 w_a + 2\left(x'''x' + y'''y'\right)v_a^3 j_a \\ &\quad \left. + 6\left(x''x' + y''y'\right)v_a w_a j_a\right]\mathrm{d}\sigma \\ &= \frac{1}{2}\int_0^{\Sigma_\xi} I\left(x', x'', x'''; y', y'', y'''; v_a, v_a', v_a''\right)\mathrm{d}\sigma. \end{aligned} \tag{A3}$$

Given the path $\boldsymbol{\xi}$, we wish to solve the problem stated in Eq. (A1), i.e., to find the optimal trajectory or, equivalently, to find $v_a^*(\sigma) = \dot{\sigma}_\xi^*(t)\Big|_{t=\tau(\sigma)}$. Note that the feasible equi-affine velocity is constrained:

$$\int_0^{\Sigma_\xi}\frac{1}{v_a}d\sigma = T.$$

Given this constraint, we introduce the constant Lagrange multiplier λ. Thus, the Euler-Poisson (E-P) equation for the functional in Eq. (A3) under the above constraint is as follows:

$$\begin{aligned} \mathrm{E{-}P}(I) &= \frac{\partial I}{\partial v_a} - \frac{d}{d\sigma}\left(\frac{\partial I}{\partial v_a'}\right) + \frac{\mathrm{d}^2}{\mathrm{d}\sigma^2}\left(\frac{\partial I}{\partial v_a''}\right) + \lambda\frac{\partial}{\partial v_a}\left(\frac{1}{v_a}\right) \\ &= v_a''' \cdot (\ldots) + v_a'' \cdot (\ldots) + \ldots v_a' \cdot (\ldots) \\ &\quad + v_a^4 \cdot \left(x'''^2 + y'''^2 - 2x''x^{(4)} - 2y''y^{(4)} + 2x'x^{(5)}\right. \\ &\quad \left. + 2y'y^{(5)}\right) - \frac{\lambda}{v_a^2} = 0. \end{aligned}$$

According to Eq. (A5), the desirable v_a for our optimal solution is constant. Consequently, all its derivatives are zero and the x and y components of the path $\boldsymbol{\xi}(\sigma) = [x(\sigma)\ y(\sigma)]$ belonging to A necessarily satisfy the following equality (Polyakov 2001, 2006, p. 24):

$$x'''^2 + y'''^2 - 2x''x^{(4)} - 2y''y^{(4)} + 2x'x^{(5)} + 2y'y^{(5)} = \text{const}$$

or, assuming that the path is six times differentiable (and differentiating both sides), $\mu = x'x^{(6)} + y'y^{(6)} = 0$.

The derivations of the necessary condition are identical for the 3D case considered below. We therefore write the necessary condition in a vector form, which can be used for both planar and spatial curves:

$$\mu = \mathbf{r}'(\sigma)\cdot\mathbf{r}^{(6)}(\sigma) = 0. \tag{A4}$$

This necessary condition may have many different solutions when considered either in 2D or in 3D. One set of 2D solutions can be recognized immediately—the parabolas from Eq. (6), which are parameterized as second-order polynomials w.r.t. σ. Indeed whenever ξ is any piece of *parabola*, $v_a^* = \text{const}$ (see Appendix C). It is important to note that the necessary condition for the path in order to satisfy the two models, Eq. (A4) or Eq. (10), must be considered together with Eq. (3).

Using Eq. (4), the sixth order derivative of the position vector can be expressed in terms of the first and second order derivatives. Correspondingly, the necessary condition in Eq. (10) can be rewritten as follows:

$$\mathbf{r}'\left(4\kappa\kappa'\mathbf{r}' + \kappa^2\mathbf{r}'' - 3\mathbf{r}''\kappa'' - \kappa'''\mathbf{r}'\right) = 0,$$

which implies

$$\mathbf{r}'^2\left(4\kappa\kappa' - \kappa'''\right) + \frac{1}{2}\left(\mathbf{r}'^2\right)'\left(\kappa^2 - 3\kappa''\right) = 0$$

and

$$\begin{aligned} &\left(3\kappa''(\sigma) - \kappa(\sigma)^2\right)\frac{\mathrm{d}}{\mathrm{d}\sigma}\log\left(\mathbf{r}'^2\right) \\ &\quad = 2\left(4\kappa(\sigma)\kappa'(\sigma) - \kappa'''(\sigma)\right)\mathbf{r}'^2. \end{aligned}$$

Finally, noting that $d\sigma = c^{1/3}ds$ and $\mathbf{r}'^2 = (\mathrm{d}\mathbf{r}/\mathrm{d}\sigma)^2 = (d\mathbf{r}/ds)^2(\mathrm{d}s/\mathrm{d}\sigma)^2 = c^{-2/3}$, we obtain a differential equation that involves Euclidian and equi-affine curvatures and their derivatives w.r.t. σ, but not position coordinates:

$$\begin{aligned} &\left(3\kappa''(\sigma) - \kappa(\sigma)^2\right)c(\sigma)^{4/3}\frac{\mathrm{d}}{\mathrm{d}\sigma}\log c(\sigma) \\ &\quad = -3\left(4\kappa(\sigma)\kappa'(\sigma) - \kappa'''(\sigma)\right). \end{aligned} \tag{A5}$$

Besides natural parameterization, equi-affine curvature can also be expressed via temporally parameterized x and y coordinates of the trajectory (Shirokov and Shirokov 1959):

$$\begin{aligned} &\kappa(\sigma(t)) \\ &\quad = \frac{3\dot{\sigma}^3\left(\dot{x}\frac{d^4y}{dt^4} - \dot{y}\frac{d^4x}{dt^4}\right) + 12\dot{\sigma}^3\left(\ddot{x}\dddot{y} - \ddot{y}\ddot{x}\right) - 5\left(\dot{x}\dddot{y} - \ddot{x}\ddot{y}\right)^2}{9\dot{\sigma}^8} \end{aligned} \tag{A6}$$

In the following we show that no planar curves other than parabolas satisfy the system of Eqs. (10) and (3), under the requirement that the simultaneous solution of Eqs. (10)

and (3) is invariant under arbitrary equi-affine transformations. That is, any equi-affine transformation of the solution constitutes a solution as well. In other words, we eliminate those solutions (e.g., circles or a specific case of logarithmic spiral mentioned in the Sect. 3) whose equi-affine transformations are no longer solutions.

A.1 Two non-invariant solutions

The minimum-jerk cost in Eq. (7) is invariant under Euclidian transformations (rotations and translations), which are a subclass of equi-affine transformations. Hence, the two-thirds power law imposes a stronger constraint on geometric invariance than the minimum jerk model. We found two non-parabolic curves that satisfy the necessary conditions defined by Eqs. (3) and (10). However, these curves, circles and logarithmic spirals (we are unaware of other solutions), while being invariant under Euclidian transformations, are not invariant under equi-affine transformations. The Euclidian curvature of circles is constant, and they can be mathematically described by

$$\begin{aligned} x(\sigma) &= x_0 + k^{-3/4}\cos\left(\sqrt{k}\sigma\right), \\ y(\sigma) &= y_0 + k^{-3/4}\sin\left(\sqrt{k}\sigma\right). \end{aligned} \tag{A7}$$

No other conic sections besides parabolas and circles, that is, neither hyperbolas nor non-circular ellipses, satisfy Eq. (10). This can be shown by direct substitution of their mathematical descriptions in terms of equi-affine arc-length (Sect. 2) into Eq. (10). Another candidate path that satisfies the necessary conditions (Eqs. (3) and (10)) is the following specific logarithmic spiral (Bright 2007):

$$\begin{aligned} x(\varphi) &= \text{const}\ \exp\left(3\varphi/\sqrt{7}\right)\cos\varphi, \\ y(\varphi) &= \text{const}\ \exp\left(3\varphi/\sqrt{7}\right)\sin\varphi, \end{aligned} \tag{A8}$$

where φ is an angle expressed in polar coordinates. However, this path is invariant under Euclidian, but not under equi-affine transformations. The radius of the Euclidian curvature ($= 1/c$) of the logarithmic spiral varies linearly with Euclidian length; the squared radius of its equi-affine curvature ($= 1/\kappa^2$) changes linearly with equi-affine length. The two non-parabolic candidate paths that satisfy the necessary conditions are not invariant under equi-affine transformations and drawing their equi-affine images according to the two-thirds power law is not necessarily maximally smooth (does not provide minimal jerk cost for such path).

A.2 A sufficient condition on the path

In formulating Eq. 10 we only derived a necessary condition that the trajectories must obey; that is, we only expressed the condition for a solution that guarantees an extremum of the jerk cost in Eq. (7), without checking whether such a solution indeed minimizes jerk. Direct calculation shows that parabolas indeed satisfy the necessary and sufficient conditions for minimizing jerk (Appendix C). Similarly, harmonic motion along circles also satisfies both the two-thirds power law and minimizes the jerk cost due to the constancy of its Euclidian curvature. However, for other possible candidate path that satisfies Eqs. (3) and (10), it may not be possible to check whether a movement with constant equi-affine speed along such path, indeed minimizes jerk. Hence we would like to derive a sufficient condition that any such geometric path should satisfy.

To do this, we used the second variation to test whether a solution of the necessary condition in Eq. (10) does provide the minimal jerk cost or whether it is just an extremal solution of the variational problem in Eq. (A3). Following Gelfand and Fomin (1963) we derive a sufficient condition for the minima of the functional in Eq. (A3), which, when satisfied, guarantees that a candidate path indeed complies with both models.

Let $h(\sigma)$ be a perturbation of the equi-affine velocity v_a along the path parameterized by σ. The function h and its derivatives up to a certain order are zeros at the boundaries of a segment: $\sigma = 0$ and $\sigma = \Sigma_\xi$. The formula for the second variation of the functional in Eq. (A3) is:

$$\begin{aligned} \delta^2 I[h] = \frac{1}{2}\int_0^{\Sigma_\zeta} \Big(& I_{v_a v_a} h^2 + 2 I_{v_a v_a'} h h' + I_{v_a' v_a'} h'^2 + 2 I_{v_a v_a''} h h'' \\ & + 2 I_{v_a' v_a''} h' h'' + I_{v_a'' v_a''} h''^2 \Big)\, \mathrm{d}\sigma, \end{aligned}$$

where $I_v = \frac{\partial}{\partial v} I$. Using integration by parts and considering zero boundary conditions on h, we have:

$$\int_0^{\Sigma_\zeta} \left(2 I_{v_a v_a'} h h'\right)\mathrm{d}\sigma = -\int_0^{\Sigma_\zeta} \left(\frac{\mathrm{d}}{\mathrm{d}\sigma} I_{v_a v_a'}\right) h^2 \mathrm{d}\sigma,$$

$$\begin{aligned} \int_0^{\Sigma_\zeta} \left(2 I_{v_a v_a''} h h''\right)\mathrm{d}\sigma &= -2\int_0^{\Sigma_\zeta} \frac{\mathrm{d}}{\mathrm{d}\sigma}\left(I_{v_a v_a''} h\right) h' \mathrm{d}\sigma \\ &= -2\int_0^{\Sigma_\zeta} \left[\frac{\mathrm{d}}{\mathrm{d}\sigma}\left(I_{v_a v_a''}\right) h h' + I_{v_a v_a'} h'^2\right]\mathrm{d}\sigma \\ &= \int_0^{\Sigma_\zeta} \left[\frac{\mathrm{d}^2}{\mathrm{d}\sigma^2}\left(I_{v_a v_a''}\right) h^2 - 2 I_{v_a v_a''} h'^2\right]\mathrm{d}\sigma, \end{aligned}$$

$$2\int_0^{\Sigma_\zeta} I_{v_a' v_a''} h' h''\mathrm{d}\sigma = -\int_0^{\Sigma_\zeta} \left(\frac{\mathrm{d}}{\mathrm{d}\sigma} I_{v_a' v_a''}\right) h'^2 \mathrm{d}\sigma.$$

Finally, the second variation can be written in the form of the sum of squares of h and its derivatives multiplied by their corresponding coefficients that do not depend on h

$$\delta^2 I[h] = \frac{1}{2}\int_0^{\Sigma_\zeta}\left[\left(I_{v_a v_a} - \frac{\mathrm{d}}{\mathrm{d}\sigma} I_{v_a v_a'} + \frac{\mathrm{d}^2}{\mathrm{d}\sigma^2} I_{v_a v_a''}\right) h^2 + \left(I_{v_a' v_a'} - 2I_{v_a v_a''}\right) h'^2 + I_{v_a'' v_a''} h''^2\right] \mathrm{d}\sigma.$$

Setting the derivatives of v_a to zero, we get

$$\begin{aligned}\delta^2 I[h] &= \int_0^{\Sigma_\zeta}\left\{2\left[x'''^2 + y'''^2 - 2x''x^{(4)} - 2y''y^{(4)} + 2x'x^{(5)} + 2y'y^{(5)}\right]h^2 \right.\\ &+ \left[9\left(x''^2 + y''^2\right) + 2\left(x'x''' + y'y'''\right) - 24\left(x''x''' + y''y'''\right)\right]h'^2\\ &\left. + \left[x'^2 + y'^2\right]h''^2\right\} v_a^3 \mathrm{d}\sigma. \end{aligned} \tag{A9}$$

The expression multiplied by h^2 is exactly twice the left-hand side of the necessary condition in Eq. (10) and is therefore constant (say c_0). The expression multiplied by h'^2 is some continuous function. Let c_1 be its minimum on the interval $[0;\ \Sigma_\xi]$. The expression multiplied by h''^2 is always positive (we assume that the curve does not contain inflection points), and we denote its minimum on the interval $[0;\ \Sigma_\xi]$ by c_2.

Let us now examine when the second variation is strictly positive, allowing the functional to achieve its minimum. We use a particular case of Poincare inequality (suggested to us by Edriss Titi). Consider some smooth enough function $u(\sigma)$ defined on the interval $[a; b]$, such that $u(a) = 0$. This function has the following properties (implied by Cauchy-Schwarz inequality):

$$\begin{aligned}u^2(\sigma) &= u^2(a) + \int_a^\sigma \left[u^2(t)\right]' \mathrm{d}t = 2\int_a^\sigma u(t)\,u'(t)\,\mathrm{d}t\\ &\le 2\left[\int_a^b u^2(t)\,\mathrm{d}t\right]^{1/2}\left[\int_a^b u'^2(t)\,\mathrm{d}t\right]^{1/2},\end{aligned}$$

which implies that $\int_a^b u^2(t)\,\mathrm{d}t \le 2(b-a)\left[\int_a^b u^2(t)\,\mathrm{d}t\right]^{1/2}\left[\int_a^b u'^2(t)\,\mathrm{d}t\right]^{1/2}$.

Finally, dividing both sides by $\left[\int_a^b u^2(t)\,\mathrm{d}t\right]^{1/2}$,

$$\left[\int_a^b u^2(t)\,\mathrm{d}t\right]^{1/2} \le 2(b-a)\left[\int_a^b u'^2(t)\,\mathrm{d}t\right]^{1/2}. \tag{A10}$$

Now, substituting the constants c_0, c_1, c_2 into Eq. (A9) and applying Eq. (A10) to the derivatives of h in Eq. (A9), we get:

$$\begin{aligned}\delta^2 I[h] &\ge v_a^3\int_0^{\Sigma_\xi}\left(c_0 h^2 + c_1 h'^2 + c_2 h''^2\right)\mathrm{d}\sigma\\ &\ge v_a^3\int_0^{\Sigma_\xi}\left(c_0 h^2 + c_1 h^2/\left(2\Sigma_\xi\right)^2 + c_2 h^2/\left(2\Sigma_\xi\right)^4\right)\mathrm{d}\sigma\\ &= v_a^3\int_0^{\Sigma_\xi} h^2\left(c_0 + c_1/\left(2\Sigma_\xi\right)^2 + c_2/\left(2\Sigma_\xi\right)^4\right)\mathrm{d}\sigma.\end{aligned}$$

The above formula implies that the second variation is positive for small enough values of Σ_ξ because c_2 is positive. Therefore, the condition in Eq. (10) is both necessary and sufficient for short path segments of any solution of the necessary condition.

Whenever c_0, which equals twice the constant from the necessary condition, is non-negative, the second variation in Eq. (A9) is bounded from below as follows:

$$\delta^2 I[h] > v_a^3 \min_{0\le\sigma\le\Sigma_\zeta}\left[9\left(x''^2+y''^2\right) + 2\left(x'x'''+y'y'''\right) - 24\left(x''x'''+y''y'''\right)\right]\cdot\int_0^{\Sigma_\zeta} h'^2\mathrm{d}\sigma.$$

The derivations for the spatial case are identical. Finally, rewriting the above inequality in the vector form, the system (see also Polyakov 2006, p. 26)

$$\begin{cases}\mathbf{r}'''^2 - 2\mathbf{r}''\cdot\mathbf{r}^{(4)} + 2\mathbf{r}'\cdot\mathbf{r}^{(5)} = c_0 \ge 0\\ \min\limits_{0\le\sigma\le\Sigma_\zeta}\left[9\mathbf{r}''^2 + 2\mathbf{r}'\cdot\mathbf{r}''' - 24\mathbf{r}''\cdot\mathbf{r}'''\right] = c_1 \ge 0\end{cases}, \tag{A11}$$

can be used as a sufficient condition for any planar or 3D path with arbitrary length Σ_ξ.

The two non-parabolic solutions, the circles in Eq. (A7) and the specific logarithmic spirals in Eq. (A8), satisfy the sufficient condition in Eq. (A11) for any value of Σ_ξ. However, as mentioned above, these two curves are not invariant under equi-affine transformations whereas parabolas are.

Appendix B: Eliminating non-invariant solutions

We show that parabolas are the only curves providing equi-affine invariant solutions of Eq. (10). The natural requirement implies that the x and y components of Eq. (10) are zeros, that is, $\mu_x = x'x^{(6)}$, $\mu_y = y'y^{(6)}$ and

$$\mu_x = \mu_y = 0. \tag{B1}$$

To make this clearer one can apply one-parametric equi-affine transformation of the form $x \to (1/\alpha)x$, $y \to \alpha y$ to the coordinates, which implies $\mu_x \to \left(1/\alpha^2\right)\mu_x$, $\mu_y \to \alpha^2\mu_y$ abolishing the necessary condition $\mu_x + \mu_y = 0$ and thus

nullifying the requirement, if μ_x and μ_y are both not zeros. The following chain of reasoning proves the uniqueness of parabolic solutions under the requirement of invariance.

From Eq. (B1), $0 = \mu_x = x'x^{(6)}$, thus $x^{(6)} = 0$, implying that $x(\sigma)$ is a 5-th order polynomial; the same holds for $y(\sigma)$. Hence, we can write

$$x(\sigma) = a_0 + a_1\sigma + a_2\sigma^2 + a_3\sigma^3 + a_4\sigma^4 + a_5\sigma^5,$$
$$y(\sigma) = b_0 + b_1\sigma + b_2\sigma^2 + b_3\sigma^3 + b_4\sigma^4 + b_5\sigma^5.$$

Substituting x and y into Eq. (3), we obtain a polynomial in σ of order 6, namely

$$\begin{aligned}&\{-2a_2b_1 + 2a_1b_2\} + 6(a_1b_3 - a_3b_1)\sigma\\ &+ \{12(a_1b_4 - a_4b_1) + 6(a_2b_3 - a_3b_2)\}\sigma^2\\ &+ \{16(a_2b_4 - a_4b_2) + 20(a_1b_5 - a_5b_1)\}\sigma^3\\ &+ \{12(a_3b_4 - a_4b_3) + 30(a_2b_5 - a_5b_2)\}\sigma^4\\ &+ 30(a_3b_5 - a_5b_3)\sigma^5 + 20(a_4b_5 - a_5b_4)\sigma^6 = 1, \quad \text{(B2)}\end{aligned}$$

which implies that the coefficients of the polynomials satisfy seven conditions. The coefficients near non-zero degrees of σ, that is near $\sigma, \sigma^2, \ldots, \sigma^6$ must be 0 and the free term needs to equal 1 to satisfy Eq. (B2).

Let us use the following notation for the six 2-dimensional vectors: $\mathbf{0} = [a_0b_0]$, $\mathbf{1} = [a_1b_1], \ldots, \mathbf{5} = [a_5b_5]$. We will prove that parabolas are the only simultaneous solutions of Eqs. (10) and (3), when equi-affine invariance is required. We do this by showing that the coefficients near degrees of σ higher than 2 are all zeros:

$$\mathbf{3} = \mathbf{4} = \mathbf{5} = [0\,0]. \quad \text{(B3)}$$

Let us write the conditions on each of the coefficients of the equi-affine velocity calculated above. On the left we write the degree of σ, to which the coefficient from Eq. (B2) corresponds. By the cross product we denote the area defined by the two vectors: $(\mathbf{r}_1 \times \mathbf{r}_2) = x_1y_2 - y_1x_2$.

$$\sigma^0 : 2(\mathbf{1} \times \mathbf{2}) = 1 \quad \text{(B4)}$$
$$\sigma^1 : 6(\mathbf{1} \times \mathbf{3}) = 0 \quad \text{(B5)}$$
$$\sigma^2 : 12(\mathbf{1} \times \mathbf{4}) + 6(\mathbf{2} \times \mathbf{3}) = 0 \quad \text{(B6)}$$
$$\sigma^3 : 16(\mathbf{2} \times \mathbf{4}) + 20(\mathbf{1} \times \mathbf{5}) = 0 \quad \text{(B7)}$$
$$\sigma^4 : 12(\mathbf{3} \times \mathbf{4}) + 30(\mathbf{2} \times \mathbf{5}) = 0 \quad \text{(B8)}$$
$$\sigma^5 : 30(\mathbf{3} \times \mathbf{5}) = 0 \quad \text{(B9)}$$
$$\sigma^6 : 20(\mathbf{4} \times \mathbf{5}) = 0. \quad \text{(B10)}$$

Let us now consider all possibilities for which Eq. (B3) is not satisfied.

- $\mathbf{3} \neq [00]$, $\mathbf{4} \neq [00]$, $\mathbf{5} \neq [00]$; Eqs. (B5), (B9) and (B10) immediately imply that the vectors $\mathbf{1}, \mathbf{3}, \mathbf{4}, \mathbf{5}$ are parallel to each other because the corresponding determinants are zero and we can use the transitivity rule: if $\mathbf{3}$ is parallel to $\mathbf{1}$ and $\mathbf{3}$ is parallel to $\mathbf{5}$, then $\mathbf{1}$ is parallel to $\mathbf{5}$, because all vectors considered are non-zero. Then Eq. (B6) implies that $\mathbf{2}$ is also parallel to all of them, which contradicts Eq. (B4).
- $\mathbf{3} \neq [00]$, $\mathbf{4} \neq [00]$, $\mathbf{5} = [00]$; Eqs. (B5)–(B8) result in all vectors being parallel, thus contradicting Eq. (B4). Cases where only $\mathbf{3}$ or only $\mathbf{4}$ is zero are proved similarly.
- $\mathbf{3} \neq [00]$, $\mathbf{4} = [00]$, $\mathbf{5} = [00]$; Eqs. (B5), (B6) imply that all vectors are parallel, again contradicting Eq. (C4). A similar proof holds for cases where only $\mathbf{4} \neq [00]$ or only $\mathbf{5} \neq [00]$.

B.1 Generalization to the 3D case

We have so far referred only to planar movements. However, planar drawings constitute a special type of movements. Three dimensional goal-directed movements, such as reaching towards a target or bringing food to the mouth, constitute a larger class of movements. Here, we mathematically identify 3D strokes for parsimonious representation of complex 3D trajectories.

It has been proposed that 3D movements conserve 3D equi-affine velocity analogous to the conservation of the 2D equi-affine velocity in 2D movements. This generalization has led to a "1/6 power law" (Pollick et al. 2008; Maoz et al. 2008). Here, by generalizing Eq. (10) to the 3D case we derive a mathematical expression for 3D paths, such that motion at a constant spatial equi-affine speeds along such paths, will also minimize jerk. The equi-affine arc-length of a 3D drawing $\mathbf{r}(t) = \{x(t), y(t), z(t)\}$ starting at time t_0 and ending at time t is

$$\sigma_3(t) = \int_{t_0}^{t} |(\dot{\mathbf{r}}\ddot{\mathbf{r}}\dddot{\mathbf{r}})|^{1/6} dt \quad \text{(B11)}$$

(Shirokov and Shirokov 1959; Guggenheimer 1977), where $(\dot{\mathbf{r}}\ddot{\mathbf{r}}\dddot{\mathbf{r}})$ denotes a mixed product of three vectors—the scalar product of one vector with the vector product of the other two, $\dot{\mathbf{r}} \cdot [\ddot{\mathbf{r}}, \dddot{\mathbf{r}}]$. Equivalently, the mixed product is equal to the volume of the parallelepiped (a cube which underwent affine transformation and thus each of its faces is a parallelogram) defined by the three vectors. Introducing the third component z, in addition to the x and y components into the derivations in Appendix A yields the necessary condition which is similar to the planar case:

$$\begin{aligned}&x'''^2 + y'''^2 + z'''^2 - 2x''x^{(4)} - 2y''y^{(4)} - 2z''z^{(4)}\\ &\quad + 2x'x^{(5)} + 2y'y^{(5)} + 2z'z^{(5)} = \text{const},\end{aligned}$$

where a prime denotes a derivative with respect to the 3D equi-affine length σ_3 defined in Eq. (B11), for time-dependent function $f' = df(t(\sigma_3))/d\sigma_3$. Differentiation of both sides leads to the vector form of the necessary condition of Eq. (10), which is the same as was derived for the planar case. The geometric interpretation is also the same as in the planar

case: $\mathbf{r}'$ is orthogonal to $\mathbf{r}^{(6)}$. Note that the necessary condition for the 3D case must be considered together with the following equality regarding parameterization by the spatial equi-affine length:

$$\left(\mathbf{r}'\mathbf{r}''\mathbf{r}'''\right) = 1. \tag{B12}$$

For a 3D path, the requirement of invariance of the solution under arbitrary spatial equi-affine transformations implies that the x, y, and z parts of Eq. (10) are zeros: $\mu_x = x'x^{(6)}$, $\mu_y = y'y^{(6)}$, $\mu_z = z'z^{(6)}$ and therefore $\mu_x = \mu_y = \mu_z = 0$ implying

$$\begin{aligned} x(\sigma_3) &= a_0 + a_1\sigma_3 + a_2\sigma_3^2 + a_3\sigma_3^3 + a_4\sigma_3^4 + a_5\sigma_3^5, \\ y(\sigma_3) &= b_0 + b_1\sigma_3 + b_2\sigma_3^2 + b_3\sigma_3^3 + b_4\sigma_3^4 + b_5\sigma_3^5, \\ z(\sigma_3) &= c_0 + c_1\sigma_3 + c_2\sigma_3^2 + c_3\sigma_3^3 + c_4\sigma_3^4 + c_5\sigma_3^5. \end{aligned}$$

Let us consider the following six 3D vectors:
$\mathbf{0} = [a_0 b_0 c_0], \mathbf{1} = [a_1 b_1 c_1], \ldots, \mathbf{5} = [a_5 b_5 c_5]$. By the mixed product $(\mathbf{r_1 r_2 r_3}) = \det\begin{pmatrix} x_1 & x_2 & x_3 \\ y_1 & y_2 & y_3 \\ z_1 & z_2 & z_3 \end{pmatrix}$ we denote the volume spanned by three 3D vectors. Substituting the equations of the fifth order polynomials into the condition on equi-affine parameterization $\left(\mathbf{r}'\mathbf{r}''\mathbf{r}'''\right) = 1$, we obtain for x, y, and z:

$$\begin{aligned} &12\,(\mathbf{123}) + 48\,(\mathbf{124})\,\sigma_3 + [72\,(\mathbf{134}) + 120\,(\mathbf{125})]\sigma_3^2 \\ &\quad + [48\,(\mathbf{234}) + 120\,(\mathbf{135})]\sigma_3^3 + [180\,(\mathbf{235}) + 240\,(\mathbf{145})]\,\sigma_3^4 \\ &\quad + 240\,(\mathbf{245})\,\sigma_3^5 + 120\,(\mathbf{345})\,\sigma_3^6 = 1. \end{aligned}$$

This immediately implies that the vectors **3**,**4**,**5** belong to the same plane, vectors **2**,**4**,**5** belong to the same plane, and vectors **1**,**2**,**4** belong to the same plane (the three planes are not necessarily the same) because they all span zero volume. The vectors **1**,**2**,**3** do not belong to the same plane, which also means that none of them is zero.

Now we consider several cases:

- The vectors **4** and **5** are not parallel to each other. This implies that the vectors **2** and **3** belong to the plane defined by vectors **4** and **5**; thus it follows that **1** also belongs to this plane. However, there is a contradiction with the Eq. (B12): the vectors **1**,**2**,**3** must span a non-zero volume.
- Vectors **4** and **5** are parallel; at least one of them is non-zero. Zero coefficients near all non-zero degrees of σ_3 are therefore impossible to achieve.
- Vectors **4** and **5** are both zero. We are left with the curves whose components are described by 3rd order polynomials satisfying $(\mathbf{123}) = 1/12$.

Spatial equi-affine transformations of the curve

$$\begin{cases} x = \sigma_3 \\ y = \frac{\sigma_3^2}{2} \\ z = \frac{\sigma_3^3}{6} \end{cases} \tag{B13}$$

represent all such equi-affine invariant solutions. This curve is called a parabolic screw line or a spatial cubic parabola; its spatial equi-affine curvature $\left(= \left(\mathbf{r}'\mathbf{r}'''\mathbf{r}^{IV}\right)\right)$ and equi-affine torsion $\left(= -\left(\mathbf{r}''\mathbf{r}'''\mathbf{r}^{IV}\right)\right)$ are zero (Shirokov and Shirokov 1959, see Polyakov 2006, pp. 172–174 for a translation of a relevant part).

As in the planar case, the two 3D invariants, spatial equi-affine curvature and equi-affine torsion, define a curve up to an equi-affine transformation. Finally, as with a planar parabola, any two cubic parabolas can be aligned by some spatial equi-affine transformation and a uniform spatial scaling.

Our theoretically-derived candidate 3D geometric primitive is a spatial cubic parabola. However, there are several differences between the planar and 3D cases. Equi-affine transformations in 3D are defined by 11 independent parameters (12 minus 1 condition constraining the determinant), while only 5 parameters are needed in the planar case. Moreover, the minimum-jerk trajectory along a parabolic screw has non-zero cost (growing linearly with the square of its equi-affine length) while a planar parabolic trajectory can have zero jerk cost. Therefore, greater smoothness and parsimony is expected for planar trajectories constructed from planar parabolas than for 3D trajectories.

Appendix C: Properties of a parabolic path w.r.t. the minimum-jerk and the two-thirds power law models

Here we show that a movement with zero jerk cost is equivalent to moving with constant equi-affine velocity along a parabola or to moving along a straight line with constant acceleration, i.e., the functions $x(t)$ and $y(t)$ are linear or quadratic functions of time.

Let the equation for a straight path (without limitations of generality) be $y = \alpha x + \beta$. Linear or quadratic parameterization of w.r.t. time leads to zero jerk cost from Eq. (7) along the trajectory. However, the equi-affine length of the straight path is zero. Therefore, straight lines in equi-affine geometry are analogous to points in Euclidean geometry. Thus, equi-affine geometry is not relevant for studies of straight movements. Note that the equi-affine velocity of drawing a straight segment is always zero.

To show how zero jerk cost follows from the constancy of the equi-affine velocity for motion along a parabolic path, we apply a temporal parameterization of the equi-affine arc

length which provides constancy of the equi-affine velocity:

$$\sigma = \alpha t + \beta, \tag{C1}$$

α and β being constants. The equation of a parabola from Eq. (6) corresponds to equi-affine transformations defined in Eq. (1) of the following coordinate expression:

$$x = \sigma, \quad y = \frac{\sigma^2}{2}, \tag{C2}$$

Thus, the functions $x = x(\sigma)$ and $y = y(\sigma)$ are always polynomials of σ of a degree not greater than 2. Substituting Eq. (C1) into Eq. (C2), we find that time parameterizations of the components $x = x(\sigma(t))$ and $y = y(\sigma(t))$ are also polynomials of at most second degree, and consequently the cost of Eq. (7) for such a movement equals zero: $J = 0$.

Now we derive the constancy of the equi-affine velocity and parabolicity of the path, given zero jerk cost of motion along that path. Let us consider that the jerk cost is zero along the trajectory. Obviously, in such a case x and y are parameterized as second-order polynomials of time:

$$J = 0 \Rightarrow \begin{bmatrix} x(t) \\ y(t) \end{bmatrix} = \begin{bmatrix} a_2 t^2 + a_1 t + a_0 \\ b_2 t^2 + b_1 t + b_0 \end{bmatrix}. \tag{C3}$$

For this type of motion we immediately find that equi-affine velocity is conserved:

$$\dot{\sigma}(t) = \sqrt[3]{\dot{x}\ddot{y} - \dot{y}\ddot{x}} = \sqrt[3]{\det \begin{pmatrix} 2a_2 t + a_1 & 2a_2 \\ 2b_2 t + b_1 & 2b_2 \end{pmatrix}}$$
$$= \sqrt[3]{\det \begin{pmatrix} a_1 & 2a_2 \\ b_1 & 2b_2 \end{pmatrix}} = \text{const}.$$

A chain of elementary transformations shows that the drawn path constitutes a segment of a parabola or a straight line. We have shown the calculations for the case corresponding to $a_2 \neq 0$. Other cases can be handled in a similar manner.

After a shift of coordinates

$$\begin{bmatrix} \tilde{x} = x - a_0 \\ \tilde{y} = y - b_0 \end{bmatrix}$$

in Eq. (C3), we obtain $t = \frac{\pm\sqrt{a_1^2 + 4a_2\tilde{x}}}{2a_2}$; therefore

$$\tilde{y} = b_2 \frac{\tilde{x} - a_1 t}{a_2} + b_1 t = \frac{b_2}{a_2}\tilde{x} - \left(\frac{b_2}{a_2} \cdot a_1 - b_1\right) t,$$

$$\tilde{y} - \frac{b_2}{a_2}\tilde{x} = \mp\left(\frac{b_2}{a_2} \cdot a_1 - b_1\right) \frac{\sqrt{a_1^2 + 4a_2\tilde{x}}}{2a_2},$$

$$4(a_2\tilde{y} - b_2\tilde{x})^2 = \left(\frac{b_2}{a_2} \cdot a_1 - b_1\right)^2 \left(a_1^2 + 4a_2\tilde{x}\right),$$

which is an equation of a parabola or a straight line.

References

Abeles M, Bergman H, Gat I, Meilijson I, Seidemann E, Tishby N, Vaadia E (1995) Cortical activity flips among quasi-stationary states. Proc Natl Acad Sci USA 92:8616–8620

Averbeck BB, Chafee MV, Crowe DA, Georgopoulos AP (2002) Parallel processing of serial movements in prefrontal cortex. Proc Natl Acad Sci USA 99:13172–13177

Averbeck BB, Crowe DA, Chafee MV, Georgopoulos AP (2003) Neural activity in prefrontal cortex during copying geometrical shapes II. Decoding shape segments from neural ensembles. Exp Brain Res 150:142–153

Ben-Shaul Y, Drori R, Asher I, Stark E, Nadasdy Z, Abeles M (2004) Neuronal activity in motor cortical areas reflects the sequential context of movement. J Neurophysiol 91:1748–1762

Biess A, Liebermann DG, Flash T (2007) Computational model for redundant human 3D pointing movements: integration of independent spatial and temporal motor plans simplifies movement dynamics. J Neurosci 48:13045–13064

Bizzi E, Mussa-Ivaldi FA, Giszter S (1991) Computations underlying the execution of movement—a biological perspective. Science 253:287–291

Bright I (2007) Motion planning through optimization. MSc Thesis, Weizmann Institute of Science

Bring J (1996) A geometric approach to compare variables in a regression model. Am Stat 50:57–62

Brockwell A, Kass RE, Schwartz AB (2007) Statistical signal processing and the motor cortex. Proc IEEE 95:881–898

Burdet E, Milner TE (1998) Quantization of human motions and learning of accurate movements. Biol Cybern 78:307–318

Calabi E, Olver PJ, Tannebaum AT (1996) Affine geometry, curve flows, and invariant numerical approximations. Adv Math 124:154–196

Calabi E, Olver PJ, Shakiban C, Tannenbaum A, Haker S (1998) Differential and numerically invariant signature curves applied to object recognition. Int J Comp Vis 26:107–135

Carpenter AF, Georgopoulos AP, Pellizzer G (1999) Motor cortical encoding of serial order in a context-recall task. Science 283:1752–1757

Craizer M, Lewiner T, Morvan J-M (2007) Combining points and tangents into parabolic polygons. J Math Imaging Vis 29:131–140

d'Avella A, Bizzi E (2005) Shared and specific muscle synergies in natural motor behaviors. Proc Natl Acad Sci USA 102:3076–3081

d'Avella A, Saltiel P, Bizzi E (2003) Combinations of muscle synergies in the construction of a natural motor behavior. Nat Neurosci 6:300–308

d'Avella A, Portone A, Fernandez L, Lacquaniti F (2006) Control of fast-reaching movements by muscle synergy combinations. J Neurosci 26:7791–7810

Dayan E, Casile A, Levit-Binnun N, Giese MA, Hendler T, Flash T (2007) Neural representations of kinematic laws of motion: evidence for action-perception coupling. Proc Natl Acad Sci USA 104:20582–20587

Dounskaia N (2007) Kinematic invariants during cyclical arm movements. Biol Cybern 96:147–163

Fishbach A, Roy SA, Bastianen C, Miller LE, Houk JC (2005) Kinematic properties of on-line error corrections in the monkey. Exp Brain Res 164:442–457

Flash T, Hogan N (1985) The coordination of arm movements: an experimentally confirmed mathematical model. J Neurosci 5:1688–1703

Flash T, Henis E (1991) Arm trajectory modifications during reaching towards visual targets. J Cogn Neurosci 3:220–230

Flash T, Hochner B (2005) Motor primitives in vertebrates and invertebrates. Curr Opin Neurobiol 15:660–666

Flash T, Handzel AA (2007) Affine differential geometry analysis of human arm movements. Biol Cybern 96:577–601
Gat I, Tishby N (1993) Statistical modeling of cell assemblies activities in associative cortex of behaving monkeys. In: Hanson SJ, Cowan JD, Giles SL (eds) Neural information processing systems, vol 5. Denver, Colorado, pp 945–953
Gat I, Tishby N, Abeles M (1997) Hidden Markov modelling of simultaneously recorded cells in the associative cortex of behaving monkeys. Netw Comput Neural Syst 8:297–322
Gelfand I, Fomin S (1963) Calculus of variations. Prentice-Hall, Englewood Cliffs
Giszter SF, Mussa-Ivaldi FA, Bizzi E (1993) Convergent force fields organized in the frog's spinal cord. J Neurosci 13:467–491
Giszter S, Patil V, Hart C (2007) Primitives, premotor drives, and pattern generation: a combined computational and neuroethological perspective. Prog Brain Res 165:323–346
Gribble PL, Ostry DJ (1996) Origins of the power law relation between movement velocity and curvature: modeling the effects of muscle mechanics and limb dynamics. J Neurophysiol 76:2853–2860
Guggenheimer HW (1977) Differential geometry. Dover, New York
Handzel A, Flash T (1999) Geometric methods in the study of human motor control. Cogn Stud 6:309–321
Handzel A, Flash T (2001) Affine invariant edge completion with affine geodesics. In: IEEE workshop on variational and level set methods, Vancouver, Canada, pp 97–103
Harris CM, Wolpert DM (1998) Signal-dependent noise determines motor planning. Nature 394:780–784
Harris CM, Wolpert DM (2006) The main sequence of saccades optimizes speed-accuracy trade-off. Biol Cybern 95:21–29
Hart CB, Giszter SF (2004) Modular premotor drives and unit bursts as primitives for frog motor behaviors. J Neurosci 24:5269–5282
Hatsopoulos NG, Paininski L, Donoghue JP (2003) Sequential movement representations based on correlated neuronal activity. Exp Brain Res 149:478–486
Hatsopoulos NG, Xu Q, Amit Y (2007) Encoding of movement fragments in the motor cortex. J Neurosci 27:5105–5114
Hebb DO (1949) The organization of behavior. Wiley, New York
Hogan N (1984) An organizing principle for a class of voluntary movements. J Neurosci 4:2745–2754
Ivanenko YP, Grasso R, Macellari V, Lacquaniti F (2002) Two-thirds power law in human locomotion: role of ground contact forces. Neuroreport 13:1171–1174
Ivanenko YP, Poppele RE, Lacquaniti F (2004) Five basic muscle activation patterns account for muscle activity during human locomotion. J Physiol 556:267–282
Ivanenko YP, Cappellini G, Dominici N, Poppele RE, Lacquaniti F. (2005) Coordination of locomotion with voluntary movements in humans. J Neurosci 25:7238–7253
Jackson A, Mavoori J, Fetz EE (2006) Long-term motor cortex plasticity induced by an electronic neural implant. Nature 444:56–60
Johnson MTV, Coltz JD, Ebner TJ (1999) Encoding of target direction and speed during visual instruction and arm tracking in dorsal premotor and primary motor cortical neurons. Eur J Neurosci 11:4433–4445
Jones LM, Fontanini A, Sadacca BF, Miller P, Katz DB (2007) Natural stimuli evoke dynamic sequences of states in sensory cortical ensembles. Proc Natl Acad Sci USA 104:18772–18777
Kargo WJ, Giszter SF (2000) Rapid correction of aimed movements by summation of force-field primitives. J Neurosci 20:409–426
Kenet T, Bibitchkov D, Tsodyks M, Grinvald A, Arieli A (2003) Spontaneously emerging cortical representations of visual attributes. Nature 425:954–956
Kording KP, Wolpert DM (2006) Bayesian decision theory in sensorimotor control. Trends Cogn Sci 10:319–326
Krebs HI, Aisen MI, Volpe BT, Hogan N (1999) Quantization of continuous arm movements in humans with brain injury. Proc Natl Acad Sci USA 96:4645–4649
Lacquaniti F, Terzuolo C, Viviani P (1983) The law relating the kinematic and figural aspects of drawing movements. Acta Psychol (Amst) 54:115–130
Levit-Binnun N, Schechtman E, Flash T (2006) On the similarities between the perception and production of elliptical trajectories. Exp Brain Res 172:533–555
Maoz U (2007) Trajectory formation and units of action, from two- to three-dimensional motion. PhD Thesis, The Hebrew University of Jerusalem
Maoz U, Berthoz A, Flash T (2008) Complex unconstrained three-dimensional arm movement and constant equi-affine speed. J Nurohysiol. doi:10.1152/jn.90702.2008
Moran DW, Schwartz AB (1999) Motor cortical representation of speed and direction during reaching. J Neurophysiol 82:2676–22692
Morasso P (1981) Spatial control of arm movements. Exp Brain Res 42:223–227
Morasso P, Mussa Ivaldi FA (1982) Trajectory formation and handwriting: a computational model. Biol Cybern 45:131–142
Mussa-Ivaldi FA, Bizzi E (2000) Motor learning through the combination of primitives. Philos Trans R Soc Lond B Biol Sci 355:1755–1769
Mussa-Ivaldi FA, Solla SA (2004) Neural primitives for motion control. IEEE J Ocean Eng 29:640–650
Nakano E, Imamizu H, Osu R, Uno Y, Gomi H, Yoshioka T, Kawato M (1999) Quantitative examinations of internal representations for arm trajectory planning: minimum commanded torque change model. J Neurophysiol 81:2140–2155
Nichols TR (1994) A biomechanical perspective on spinal mechanisms of coordinated muscular action: an architecture principle. Acta Anatomica 151:1–13
Osu R, Kamimura N, Iwasaki H, Nakano E, Harris CM, Wada Y, Kawato M (2004) Optimal impedance control for task achievement in the presence of signal-dependent noise. J Neurophysiol 92:1199–1215
Paninski L, Shoham S, Fellows MR, Hatsopoulos NG, Donoghue JP (2004) Superlinear population encoding of dynamic hand trajectory in primary motor cortex. J Neurosci 24:8551–8561
Pollick FE, Sapiro G (1997) Constant affine velocity predicts the 1/3 power law of planar motion perception and generation. Vis Res 37:347–353
Pollick FE, Maoz U, Handzel AA, Giblin PJ, Sapiro G, Flash T (2008) Three-dimensional arm movements at constant equi-affine speed. Cortex (in press). doi:10.1016/j.cortex.2008.03.010
Polyakov F (2001) Analysis of monkey scribbles in the framework of models of planar hand motion. MSc Thesis, Weizmann Institute of Science. http://www.wisdom.weizmann.ac.il/~felix/texts/polyakov_thesis_msc.pdf (cited on June 18, 2008)
Polyakov F (2006) Motion primitives and invariants in monkey scribbling movements: analysis and mathematical modeling of movement kinematics and neural activities. PhD Thesis, Weizmann Institute of Science. http://www.wisdom.weizmann.ac.il/~felix/texts/polyakov_thesis_phd.pdf (cited on May 29, 2008)
Polyakov F, Flash T, Abeles M, Ben-Shaul Y, Drori R, Nadasdy Z (2001) Analysis of motion planning and learning in monkey scribbling movements. In: Meulenbrouk R, Steenbergen B (eds) Proceedings of the 10th biennial conference of the International Graphonomics Society. The University of Nijmegen, Nijmegen, The Netherlands. pp 78–83. http://www.wisdom.weizmann.ac.il/~felix/texts/IGS2001.pdf (cited on June 18, 2008)
Reina GA, Schwartz AB (2003) Eye–hand coupling during closed-loop drawing: Evidence of shared motor plans? Hum Mov Sc 22:137–152

Richardson MJ, Flash T (2002) Comparing smooth arm movements with the two-thirds power law and the related segmented-control hypothesis. J Neurosci 22:8201–8211

Rohrer B, Hogan N (2003) Avoiding spurious submovement decompositions: a globally optimal algorithm. Biol Cybern 89:190–199

Rohrer B, Hogan N (2006) Avoiding spurious submovement decompositions II: a scattershot algorithm. Biol Cybern 94:409–414

Sanger TD (2000) Human arm movements described by a low-dimensional superposition of principal components. J Neursci 20:1066–1072

Schaal S, Sternad D (2001) Origins and violations of the two-thirds power law in rhythmic three-dimensional arm movements. Exp Brain Res 136:60–72

Schwartz AB (1992) Motor cortical activity during drawing movements—single-unit activity during sinusoid tracing. J Neurophysiol 68:528–541

Schwartz AB (1994) Direct cortical representation of drawing. Science 265:540–542

Schwarz G (1978) Estimating the dimension of a model. Ann Stat 6:461–464

Scott SH (2004) Optimal feedback control and the neural basis of volitional motor control. Nat Rev Neurosci 5:532–546

Sergio LE, Hamel-Paquet C, Kalaska JF (2005) Motor cortex neural correlates of output kinematics and kinetics during isometric-force and arm-reaching tasks. J Neurophysiol 94:2353–2378

Shirokov PA, Shirokov AP (1959) Affine differential geometry (in Russian). GIFML, Moscow

Soechting JF, Terzuolo CA (1987a) Organization of arm movements. Motion is segmented. Neuroscience 23:39–51

Soechting JF, Terzuolo CA (1987b) Organization of arm movements in three-dimensional space. Wrist motion is piecewise planar. Neuroscience 23:53–61

Sosnik R, Hauptmann B, Karni A, Flash T (2004) When practice leads to co-articulation: the evolution of geometrically defined movement primitives. Exp Brain Res 156:422–438

Spivak MA (1999) A comprehensive introduction to differential geometry. Publish or Perish Inc., Berkeley

Stark E, Drori R, Asher I, Ben-Shaul Y, Abeles M (2007) Distinct movement parameters are represented by different neurons in the motor cortex. Eur J Neurosci 26:1055–1066

Sternad D, Schaal S (1999) Segmentation of endpoint trajectories does not imply segmented control. Exp Brain Res 124:118–136

Tanaka H, Krakauer JW, Qian N (2006) An optimization principle for determining movement duration. J Neurophysiol 95:3875–3886

Thoroughman KA, Shadmehr R (2000) Learning of action through adaptive combination of motor primitives. Nature 407:742–747

Todd JT, Oomes AH, Koenderink JJ, Kappers AM (2001) On the affine structure of perceptual space. Psychol Sci 12:191–196

Todorov E (2004) Optimality principles in sensorimotor control. Nat Neurosci 7:907–915

Todorov E, Jordan MI (1998) Smoothness maximization along a predefined path accurately predicts the speed profiles of complex arm movements. J Neurophysiol 80:696–714

Todorov E, Jordan MI (2002) Optimal feedback control as a theory of motor coordination. Nat Neurosci 5:1226–1235

Torres E, Andersen R (2006) Space-time separation during obstacle-avoidance learning in monkeys. J Neurophysiol 96:2613–2632

Tresch MC, Saltiel P, Bizzi E (1999) The construction of movement by the spinal cord. Nat Neurosci 2:162–167

Uno Y, Kawato M, Suzuki R (1989) Formation and control of optimal trajectory in human multijoint arm movement—minimum torque-change model. Biol Cybern 61:89–101

Viviani P (1986) Do units of motor action really exist?. In: Heuer H, Fromm C (eds) Generation and modulation of action patterns. Springer, Berlin pp 201–216

Viviani P, Cenzato M (1985) Segmentation and coupling in complex movements. J Exp Psychol Hum Percept Perform 11:828–845

Viviani P, Flash T (1995) Minimum-jerk, two-thirds power law, and isochrony: converging approaches to movement planning. J Exp Psychol Hum Percept Perform 21:32–53

Viviani P, Stucchi N (1992) Biological movements look uniform: evidence of motor-perceptual interactions. J Exp Psychol Hum Percept Perform 18:603–623

Wu W, Black MJ, Mumford D, Gao Y, Bienenstock E, Donoghue JP (2004) Modeling and decoding motor cortical activity using a switching Kalman filter. IEEE Trans Biomed Eng 51:933–942

van Zuylen EJ, Gielen CC, van der Gon Denier JJ (1988) Coordination and inhomogeneous activation of human arm muscles during isometric torques. J Neurophysiol 60:1523–1548